Journal of Applied Polymer Science

WILEY

Applied Polymer SCIENCE

RESEARCH ARTICLE OPEN ACCESS

Development of Chitosan/PVA Nanofibrous Membranes for Efficient Removal of *Microcystis aeruginosa*

Cynthia Ribeiro Guimarães[1,2] | Valderi Duarte Leite[3] | Raquel Santos Leite[2] | Maria Virgínia da Conceição Albuquerque[3] | Ingridy Dayane dos Santos Silva[4] | Renate Maria Ramos Wellen[5] | Gelmires de Araújo Neves[2] | Valmor Roberto Mastelaro[6] | Romualdo Rodrigues Menezes[2]

[1]Graduate Program in Materials Science and Engineering, Federal University of Campina Grande, Campina Grande, Brazil | [2]Laboratory of Materials Technology, Department of Materials Engineering, Federal University of Campina Grande, Campina Grande, Brazil | [3]Department of Environmental Sanitary Engineering, State University of Paraíba, Campina Grande, Brazil | [4]Department of Chemistry, Federal University of Paraíba, João Pessoa, Brazil | [5]Department of Materials Engineering, Federal University of Paraíba, João Pessoa, Brazil | [6]IFSC—University of São Paulo, São Carlos, São Paulo, Brazil

Correspondence: Cynthia Ribeiro Guimarães (cynthia.ribeiro@live.com) | Romualdo Rodrigues Menezes (romualdo.rodrigues@professor.ufcg.edu.br)

Received: 27 January 2025 | **Revised:** 14 July 2025 | **Accepted:** 16 July 2025

Funding: The authors would like to thank CNPq (grant no. 141518/2021-9, 420004/2018-1, 309771/2021-8 and 309234/2020-4), FAPESQ (grant term no. 3064/2021 and grant term no. 036/2023/PRONEX) and FAPESP (grant no. 2013/07296-2) for financial support.

Keywords: adsorption | blends | composites

ABSTRACT

In this study, chitosan/poly(vinyl alcohol) (CS/PVA) polymeric nanofibers were produced using the Air-Heated Solution Blow Spinning (A-HSBS) method and applied for the efficient removal of *Microcystis aeruginosa* from contaminated water. Nanofibers were fabricated with chitosan contents ranging from 10 to 50 wt% and subsequently characterized by scanning electron microscopy (SEM), transmission electron microscopy (TEM), Fourier transform infrared spectroscopy (FTIR), X-ray photoelectron spectroscopy (XPS), X-ray diffraction (XRD), thermogravimetric analysis (TG), differential scanning calorimetry (DSC), and apparent porosity measurements. The materials exhibited a highly porous, three-dimensional, cotton-wool-like fibrous morphology, with porosity exceeding 90%. The nanofibers presented smooth surfaces, randomly oriented structures, and average diameters between 230 ± 73 nm and 340 ± 102 nm. Incorporation of chitosan reduced the semicrystalline nature of PVA while enhancing the thermal stability of the fibers. Under optimized conditions—nanofibers containing 10 wt% chitosan and a fiber dosage of 20 mg per 10 mL of contaminated water—the system achieved up to 90% removal of *Microcystis aeruginosa* within 20 min. Additionally, MC-LR concentrations below 0.01 μg/L were detected following cyanobacterial removal. These findings demonstrate the potential of A-HSBS-produced CS/PVA nanofibers as a rapid, effective, and scalable treatment alternative for addressing cyanobacterial contamination in aquatic environments.

1 | Introduction

Eutrophication in the aquatic environment is a problem faced worldwide due to the proliferation of cyanophyceous algae (cyanobacteria) [1] with the rise in global temperatures. The intensification of cyanobacteria growth occurs through the deposition of nutrients and climate warming [2]. Studies indicate that by 2050, there will be at least a 20% increase in drinking water sources contaminated with harmful algal blooms [3].

The primary challenge posed by the presence of *Microcystis aeruginosa* in water resources is the release of microcystins (cyanotoxins) following cell rupture (cell lysis). Cyanotoxins are toxic to the liver and nervous system and can cause liver failure

[Correction added on October 21, 2025, after first online publication: Valderi Leite Duarte has been updated as Valderi Duarte Leite].

and brain damage [4–6]. The same toxin can present different variants, significantly altering its toxicity. Additionally, the simultaneous occurrence of different cyanotoxins can potentiate their toxic effects, generating complex interactions that cannot be predicted based on data obtained from individual toxins [7]. Thirty-seven congeners of microcystins (MC) with reported lethal dose (LD_{50}) values have been described, with microcystin-LR (MC-LR) being one of the most toxic, presenting an LD_{50} value of 50 μg/kg in mice by intraperitoneal injection [8]. MC-LR acts as a potent inhibitor of protein phosphatases 1 (PP1) and 2A (PP2A), with inhibitory concentrations ranging from 0.1 to 1 nM in vitro [7, 9].

Microcystis aeruginosa is the dominant species in cyanobacterial blooms and the most common alga in freshwater environments worldwide. It features a spherical shape with diameters that can range between 4.0 and 9.4 μm and the ability to move freely in a vertical direction [2, 10, 11]. The toxin produced by *Microcystis aeruginosa* is Microcystin Leucine-Arginine (MC-LR), the most toxic cyanotoxin among the MC [12]. The World Health Organization (WHO) recommends a concentration of $1\,\mu g/L^{-1}$ of MC-LR as a reference value for drinking water [6].

Cyanobacteria can be removed through physical, chemical, and biological treatments [13]. Additionally, methods such as the application of chlorine, algaecides, or hydrogen peroxide can be employed to mitigate the rapid proliferation of harmful algae. However, these removal processes are subject to significant limitations, including high operational or energy costs as well as notable ecological impacts [12, 14]. Moreover, cyanotoxins can be released during or as a consequence of these treatments, further aggravating the problem of water contamination.

Cyanobacteria and cyanotoxins adsorption using nanostructured materials are an alternative to retaining both the bacteria and the toxin. As a result, recent studies [12, 15, 16] have focused on developing efficient materials that can serve as "membranes" for the adsorption of cyanobacteria and cyanotoxins. In this context, nanofibrous materials emerge as an environmentally friendly alternative with high adsorptive capacity [15, 17] showing promise for treating water contaminated with cyanobacteria.

Among the polymeric materials applied for the removal of *Microcystis aeruginosa*, chitosan stands out, with adsorption predominantly occurring through electrostatic interactions between protonated amino groups and the negatively charged cell surface of the cyanobacterium [15, 18]. Chitosan-modified cotton fibers have demonstrated superior efficiency due to the introduction of positive charges on the fiber surface, combined with the large surface area provided by the fibrous structure of the material. Cotton fibers subjected to alkaline pretreatment followed by chitosan functionalization achieved 95% removal of *M. aeruginosa* cells within 12 h, indicating that the increased availability of anionic groups on the fiber surface favors electrostatic interactions with the $-NH3^{+}$ groups of chitosan under appropriate pH conditions [15]. Additionally, chitosan-functionalized nanobubbles promoted the inactivation of 73.16% ± 2.23% of the cells by disrupting nutrient transport across the cell membrane [14]. Other materials, such as hydrogels composed of chemically modified gelatin, graphene nanoparticles, and PVA, also exhibited high performance, achieving removal rates of 90% for cells, 75% for chlorophyll-a, and reductions of 63% and 43% in turbidity and visible color, respectively, after 19 h of treatment. In this case, removal occurred through the formation of small cellular aggregates followed by cell lysis, with the kinetic data fitting best to the Elovich model, suggesting a possible chemisorption mechanism [19].

Polymeric blends of chitosan/polyvinyl alcohol (PVA) with nanofiber structures and low chitosan content have recently demonstrated high efficiency in treating water contaminated by dyes or heavy metals [20–22]. However, no study has evaluated the potential of this type of material for removing *Microcystis aeruginosa*.

Chitosan (CS) is utilized in water treatment as a flocculant and coagulant agent for cyanobacteria, with the ability to retain extracellular cyanotoxins, such as microcystin-LR [3, 12, 23]. On the other hand, PVA is a nontoxic synthetic polymer that exhibits hydrophilicity and has been utilized in water treatment [24, 25]. The blend of polyvinyl alcohol (PVA) and chitosan enhances the mechanical strength of chitosan systems and improves the stability in aqueous systems of PVA bodies. Moreover, the presence of PVA reduces the repulsive forces during the spinning of chitosan-based fibers, thereby optimizing the spun process and producing more homogeneous fibers [20, 26–28].

Studies have reported the production of chitosan/PVA fibers by electrospinning [29–31], centrifugal spinning [32], and solution blowing [26, 33]. However, the production of PVA/chitosan fibers containing a high percentage of chitosan (more than 20% by weight) remains a challenge, despite the high potential of this system in adsorption processes and water treatment.

Thus, this study aims to synthesize PVA/chitosan fibrous systems with a high chitosan content through the air-heated solution blow spinning (A-HSBS) methodology, a recent adaptation of solution blow spinning (SBS) [34]. It is worth highlighting that the A-HSBS method differs from the conventional Solution Blow Spinning (SBS) technique by incorporating heated air into the process, resulting in optimized cotton-like 3D morphologies and structures for applications in tissue engineering, catalysis, and other fields [35–39]. The materials produced using this method exhibit high interconnected porosity, surface microroughness, and enhanced physicochemical properties, such as the induction of oxygen vacancies and specific coloration, thermal stabilization at low temperatures, crystallization control [38], as well as superior electrochemical performance in oxygen evolution reaction (OER) processes [37].

In addition to the production of these fibers, the study will assess their potential for removing *Microcystis aeruginosa* from water by evaluating their adsorptive capacity. This dual focus on both the synthesis of the fibers and their practical application in microalgae removal will provide valuable insights into their efficacy for environmental remediation. It is important to emphasize that, to the best of our knowledge, this study is the first to investigate the use of A-HSBS-produced chitosan/PVA nanofibers for removing *Microcystis aeruginosa* from contaminated water.

2 | Methods and Materials

2.1 | Materials

Chitosan (molecular weight of 50,000–190,000 Da and Deacetylation > 75%) and Polyvinyl alcohol (PVA) (molecular weight of 89,000–98,000 Da and 99+% hydrolyzed), in powder forms, were obtained from Sigma-Aldrich. Glacial acetic acid (> 99.5%) (Química Moderna) and glutaraldehyde solution (Grade II, 25% in H_2O) (Sigma-Aldrich) were used during the production of the fibrous materials.

2.2 | CS/PVA Fibers Production

PVA was dissolved in distilled water (6.6% w/v) under constant stirring at 60°C. The solution was acidified using acetic acid. Then, chitosan was added (from 10 to 50 wt% in relation to the PVA amount) under constant stirring at 60°C. The nomenclature of the samples in this study is PVA, 10% CS/PVA, 20% CS/PVA, 30% CS/PVA, 40% CS/PVA, and 50% CS/PVA, corresponding to chitosan proportions of 0%, 10%, 20%, 30%, 40%, and 50%, respectively, in the chitosan/PVA system.

The solutions were spun using an SBS concentric nozzle [34] at a rate of 6.0^{-1} mL/h. An air pressure at 0.41 MPa and a working distance of 200 mm were used in the study. For the spinning process, heat guns were used to assist in solvent evaporation (A-HSBS), as detailed in previous work [35]. The fibers were collected in a chamber at 50°C. The humidity in the spinning chamber was below 30%.

Cotton wool-like CS/PVA fibers were then collected and placed into a closed chamber, where they were exposed to glutaraldehyde vapor. The chamber was heated at 50°C for 168 h for crosslinking of polyvinyl alcohol (PVA) by glutaraldehyde vapor. The excess glutaraldehyde vapor (condensed on the sample) was removed using a vacuum for 24 h.

2.3 | Characterization

Fiber's morphology was characterized by scanning electron microscopy (SEM) (TESCAN, VEGA 4), with fiber diameter measured using the Image J software (National Institutes of Health, USA). At least 100 fibers from different samples were used to determine the mean diameter.

For SEM analysis following the adsorption of cyanobacteria, a methodology adapted from [40] was used. Cellular dehydration occurred with ethyl alcohol solutions at 50%, 70%, 80%, 90%, 95%, and 100% for 15 min each. Subsequently, the sample is subjected to the freeze-drying process and sent for analysis using a FEG-SEM (Tescan, MIRA 4).

Transmission electron microscope (TEM) (Tecnai G2 Spirit TWIN). For TEM observation, the fibers were deposited by dispersion on the TEM copper mesh.

Fibers were characterized by Fourier Transform Infrared Spectroscopy (FTIR) (Shimadzu, IRAffinity-1/1S), using KBr pellets with 0.6 wt% fibers, from 4000 to 400 cm^{-1}, with 32 scans and a resolution of 4 cm^{-1}; and by X-ray diffraction (XRD) (Shimadzu, XRD-6000), using Cu Kα (40 kV/30 mA) under fixed-time mode, with a step of 0.02°C and a fixed time of 6 s.

X-ray photoelectron spectroscopy (XPS) measurements were performed using a Scienta Omicron ESCA+ spectrometer equipped with a high-performance hemispherical analyzer (EAC2000) and a monochromatic Al Kα radiation source (photon energy = 1486.6 eV). Data analysis was carried out using CASA XPS software.

Thermogravimetric analysis (TGA) (Shimadzu, DTG-60H) was performed under N_2 atmosphere with a heating rate of 10°C/min^{-1} and differential scanning calorimetry (DSC) analysis was performed in DSC25 from TA Instruments (EUA) using a closed aluminum pan under a nitrogen gas flow of 50 mL/min. Samples of approximately 3 mg were heated from 20°C to 250°C.

The contact angle was measured using SEO brand equipment, model Phenix I. Images of the distilled water droplet were captured every 200 ms in static mode on a homogeneous surface of the material sample at 20°C.

The apparent porosity of the cotton wool-like 3D membranes was determined using the Archimedes' principle, as per other studies [41, 42] and ethyl alcohol as the solvent. The measurements were performed in triplicate.

Water uptake was determined using a methodology reported in the literature [43, 44]. Four milligrams of the material was weighed (W_0) and immersed in 30 mL of distilled water for 24 h. After this period, the samples were dried on a filter paper and weighed (W_i). The value of water absorption is calculated as the percentage of mass increase [43]. The experiment was carried out in triplicate.

2.4 | Cultivation of the *Microcystis aeruginosa* and Removal Test

Microcystis aeruginosa was cultivated with the strain registered in the World Date Center for Microorganisms 835. The replication of these cyanobacteria was performed according to the methodology reported in the literature [45], with the following conditions: A 12 h photoperiod with illumination of 1200 lux, at 24°C. The culture medium for *Microcystis aeruginosa* was ASM-1 [45]. Cell density was determined with an optical microscope (Coleman, NIB-100 INF), by the method described by Utermöhl [46].

First, in the removal experiments for *Microcystis aeruginosa* were evaluated using the turbidity parameter (Hanna, HI98703). The amount of adsorbent (5, 10 and 20 mg) and the contact time (5, 20 and 60 min) were evaluated. With *Microcystis aeruginosa* a fixed volume of 10 mL of *Microcystis aeruginosa* suspension, the fibers were deposited under the suspension at a temperature of 25°C and a rotation speed of 70 rpm. Then, the concentration of *Microcystis aeruginosa* was measured using UV–Vis spectroscopy (KASVI), following the methodology described in the literature [12] at a wavelength of 680 nm. The algae capture

efficiency (%CE) was obtained as reported in the literature and described in Equation (1) [12]:

$$\%\,\mathrm{CE} = \frac{C_i - C_f}{C_i} \times 100 \quad (1)$$

where, C_i and C_f are the optical density at 680 nm at the start and end time, respectively.

To *Microcystis aeruginosa* determine the correlation between optical density (OD) and dry weight of *Microcystis aeruginosa* cells (DWM), algal suspensions with varying concentrations were measured for OD using a V-visible spectrophotometer, as reported in the literature [12]. The concentration of the algae ($g\,L^{-1}$) was determined by dry cell weight (DWM). To determine DWM, 20 mL of deionized water was passed through Macherey-Nagel model 85/70 BF glass microfiber filters with 0.6 μm retention using a vacuum pump, followed by drying at 105°C under a porcelain plate to achieve a constant weight (m_A). Subsequently, 20 mL of the algae suspension was passed through the filter, placed under the porcelain plate, and heated to 105°C until a constant weight is obtained. The dry weight of the cells ($g\,L^{-1}$) was calculated according to Equation (2):

$$\mathrm{DWM} = \frac{m_B - m_A}{V} \quad (2)$$

where m_A and m_B are the masses of the dry filter and plate assembly before and after filtration, respectively, and V is the volume of the seaweed suspension used.

The variation in microcystin concentration after the removal tests was quantified using an Enzyme-Linked Immunosorbent Assay (ELISA) with the MC-ADDA kit (Abraxis). For this, the samples were collected at the end of the removal experiments, centrifuged, and an aliquot of the supernatant was taken for analysis. All measurements were performed in duplicate, strictly following the manufacturer's protocol.

3 | Results and Discussion

3.1 | Morphological Characterization of CS/PVA

Continuous fibers with smooth surfaces and random orientations, regardless of the chitosan concentration, were observed in the developed cotton-like fibrous materials (Figure 1). The fibers obtained in this study presented mean diameters of 231 ± 85 nm, 241 ± 73 nm, 230 ± 73 nm, 340 ± 102 nm, 315 ± 197 nm, and 254 ± 96 nm for PVA, 10% CS/PVA, 20% CS/PVA, 30% CS/PVA, 40% CS/PVA, and 50% CS/PVA, respectively. The morphology of the fibers is similar to that observed in electrospun PVA/CS fibers [20]; however, the diameters were smaller than those reported in the literature for solution blow spun PVA/CS systems [33]. Moreover, no study (using electrospinning or SBS) reported success in the production of CS/PVA fibers with a high amount of chitosan, such as 50%.

The PVA, 10% CS/PVA, and 20% CS/PVA systems exhibited similar mean fiber diameters ($p > 0.05$). However, the mean diameter increased in the 30% CS/PVA and 40% CS/PVA materials ($p < 0.05$), with no statistical difference observed between these two groups ($p = 0.6007$). This behavior is consistent with findings in the literature [41]. Notably, the mean diameter decreased with an increase in chitosan content from 40% to 50%, which is contrary to expectations based on the electrospinning literature [47].

The increase in chitosan content raises the viscosity of the spinning solution, which generally contributes to larger diameters, explaining the 30% and 40% increase in the diameter of CS/PVA fibers.

However, studies on A-HSBS producing ceramic fibers [37] have observed that slow solvent evaporation rates can lead to reduced fiber diameters, whereas higher evaporation rates tend to increase diameter and result in more porous materials. Thus, at higher viscosities (such as in 50% CS/PVA system), solvent permeability and drying processes may be impaired, leading to reduced evaporation rates. This phenomenon may explain the smaller fiber diameters observed in the 50% CS/PVA system compared to the 30% and 40% chitosan systems.

To elucidate the location of chitosan in the fiber, transmission electron microscopy (TEM) analysis was performed (Figure 2). It is observed that chitosan is partially deposited on PVA fiber in spherical form. Chitosan has a uniform spherical shape with gauge dimensions that can range from 0.3 to 100 nm. According to Zhang et al. [48], TEM-EDS analysis revealed phase segregation in the CS/PVA fibers, indicating that chitosan was distributed within the fibers and at defect sites, whereas PVA was distributed in a separate phase. A similar observation was reported in another study by Adibzadeh et al. [49], in which the presence of chitosan on the fiber surface facilitated the deposition of Ag nanoparticles on the surface of the nanofibers.

Studies reported by Liu et al. [33] using SBS to produce PVA/CS (CS with an average molecular weight) fibers and using ethylene glycol diglycidyl ether as a crosslinking agent obtained fibers with diameters ranging from 437 to 475 nm. In another study [26], a variation of SBS methodology, denoted air-blow, was used to produce chitosan/PVA fibers with diameters ranging from 1.5 to 4 μm. Thus, in the present work, thinner fibers were obtained when A-HSBS was applied to produce CS/PVA fibers.

Figure 3 presents FTIR spectra of CS/PVA fibers. The vibrations between 3600 and 3100 cm^{-1}, Region I in Figure 2, are assigned to stretching vibrations of the —OH (PVA) and —NH_2 (CS) groups [50]. Studies [51, 52] have depicted that the interaction between chitosan and PVA causes the formation of an amide bond in this region. In this study, a displacement of vibration from 3412 to 3380 cm^{-1} was observed in 50% CS/PVA.

In the region between 3070 and 2700 cm^{-1} (Region II), vibrations are associated with the symmetry of CH_2 and the asymmetry of C—H in the polymer chain [51, 53, 54]. In Region III, the vibration at 1551–1563 cm^{-1} is related to the symmetrical deformation of —NH_3, resulting from the ionization of primary amino groups in the acid medium [55], occurring in all samples with CS. The vibration at 1430 cm^{-1} is attributed to the stretching of

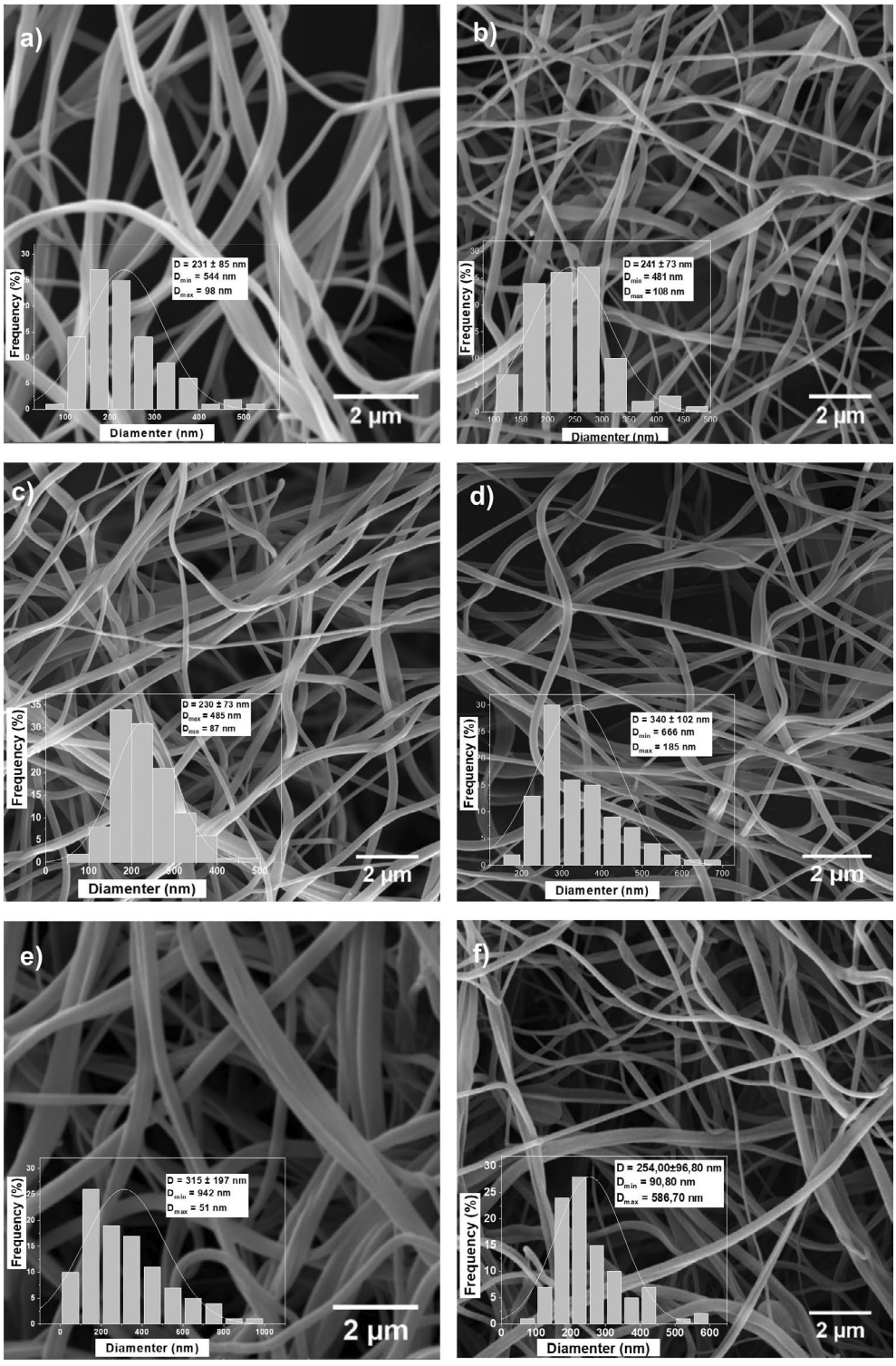

FIGURE 1 | SEM micrographs and graphics distributions of diameters (a) PVA, (b) 10% CS/PVA, (c) 20% CS/PVA, (d) 30% CS/PVA, (e) 40% CS/PVA and (f) 50% CS/PVA.

the chitosan amino group [51]. The 40% CS/PVA and 50% CS/PVA compositions exhibited a vibration at 1380 cm^{-1}, which is attributed to the C—H bond of the CH_2OH group in chitosan, resulting from the hydrogen bond with PVA [51]. At 1212 and 906 cm^{-1} (Region IV) vibrations occur related to the saccharide structure of chitosan and at 1022 cm^{-1} to the stretching of the C—O bond [21, 51]. The vibration that occurs at 844 cm^{-1} refers to the vibrations of the flexures of the C—H bonds of the PVA molecule [56].

Figure 2 shows the confirmation of the crosslinking of the CS/PVA samples with glutaraldehyde vapor, evidenced by the shifts in the vibrations from 1611 to 1653 cm^{-1} and from 1538 to 1559 cm^{-1}. These shifts correspond to the stretching of the

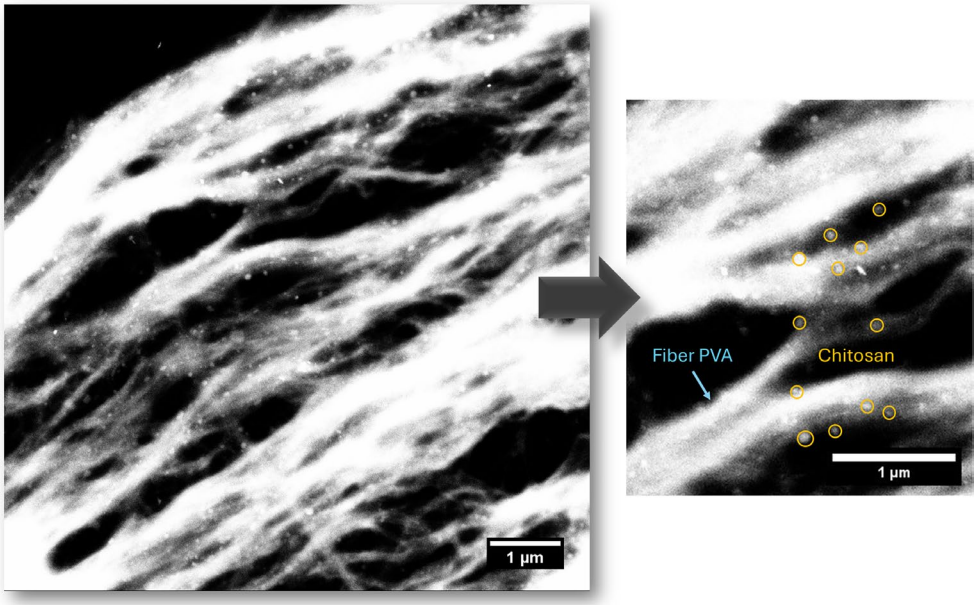

FIGURE 2 | TEM image showing the morphology of 50% CS/PVA nanofibers. [Color figure can be viewed at wileyonlinelibrary.com]

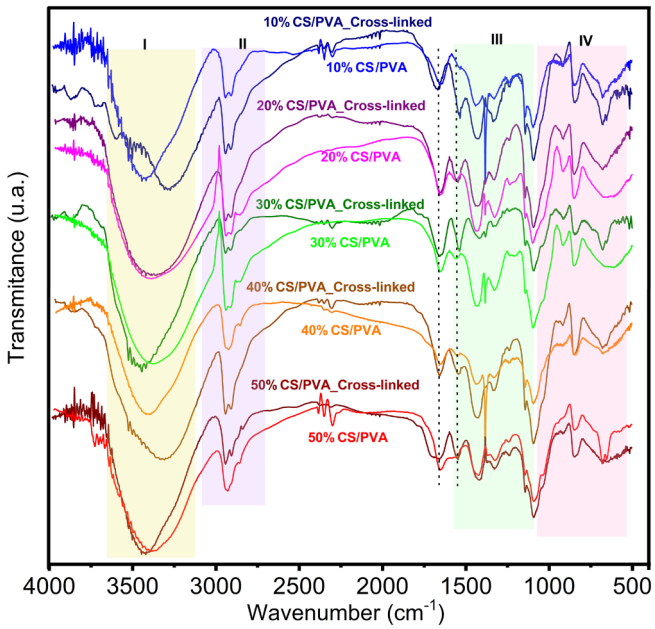

FIGURE 3 | FTIR spectra of CS/PVA before cross-linking and CS/PVA after cross-linking with glutaraldehyde. [Color figure can be viewed at wileyonlinelibrary.com]

imine group (C═N), resulting from the reaction between the aldehyde groups (glutaraldehyde) and the amine groups (chitosan) [57, 58].

The crosslinking agent forms chemical bonds that join the polymer chains, reducing the solubility of PVA while improving its mechanical and thermal properties [59, 60]. Glutaraldehyde was used for crosslinking PVA fibers with chitosan [61], aiming to improve membrane adsorption efficiency and enhance stability in an aqueous medium.

To elucidate the chemical modification of CS/PVA nanofibers crosslinked with glutaraldehyde vapor, X-ray photoelectron spectroscopy (XPS) analyses were performed before and after the modification process for the 50% CS/PVA composition (Figure 4). As shown in Figure 4, the C1s, N1s, and O1s peaks correspond to the characteristic structure of CS/PVA [62–64]. The high-resolution spectra revealed specific changes in the binding energies of the C1s and N1s regions after crosslinking. The C1s peak, initially observed at 288.6 eV and attributed to O—C═O groups, shifted to 286.7 eV, corresponding to C—O—C bonds. In the N1s region, the binding energy at 399.4 eV, assigned to amine ($C—NR_2$, where R═C, H) and/or nitrogen in aromatic rings (such as pyridine), remained unchanged. In contrast, the signal at 397.4 eV, associated with pyridinic nitrogen (pyridinic-N), disappeared. Concurrently, a new peak appeared at 401.2 eV, attributed to imide groups (C═O)—N—(C═O) or N—(C═O)—O—. This result suggests the occurrence of crosslinking reactions involving the amino groups of chitosan, promoted by the interaction with glutaraldehyde [63, 65]. Therefore, the modifications observed in the N1s region indicate the formation of C═N species and other nitrogen-containing structures. The alteration in the N1s spectral profile observed in this study reinforces the effective crosslinking of the nanofibers. Additionally, it was found that the carbon content increased from 70.6% to 73.2%, which may be associated with the introduction of carbon-containing groups from glutaraldehyde, resulting from interactions between the —OH and $—NH_2$ groups of the CS/PVA matrix and the C═O groups of the crosslinking agent [66].

PVA fibers exhibited three characteristic X-ray reflection peaks at $2\theta = 11.6°$, 19.79°, and 40.8° (Figure 5), as observed in other studies [20, 67–69], and corresponding to ICDD card No. [00-061-1401]. This molecular arrangement enables the material to preferentially crystallize in an orthorhombic unit cell. The wide and diffuse bands of PVA are characteristic of partially acoustic structures; the semicrystalline structure is formed by means of intra- and intermolecular hydrogen bonds

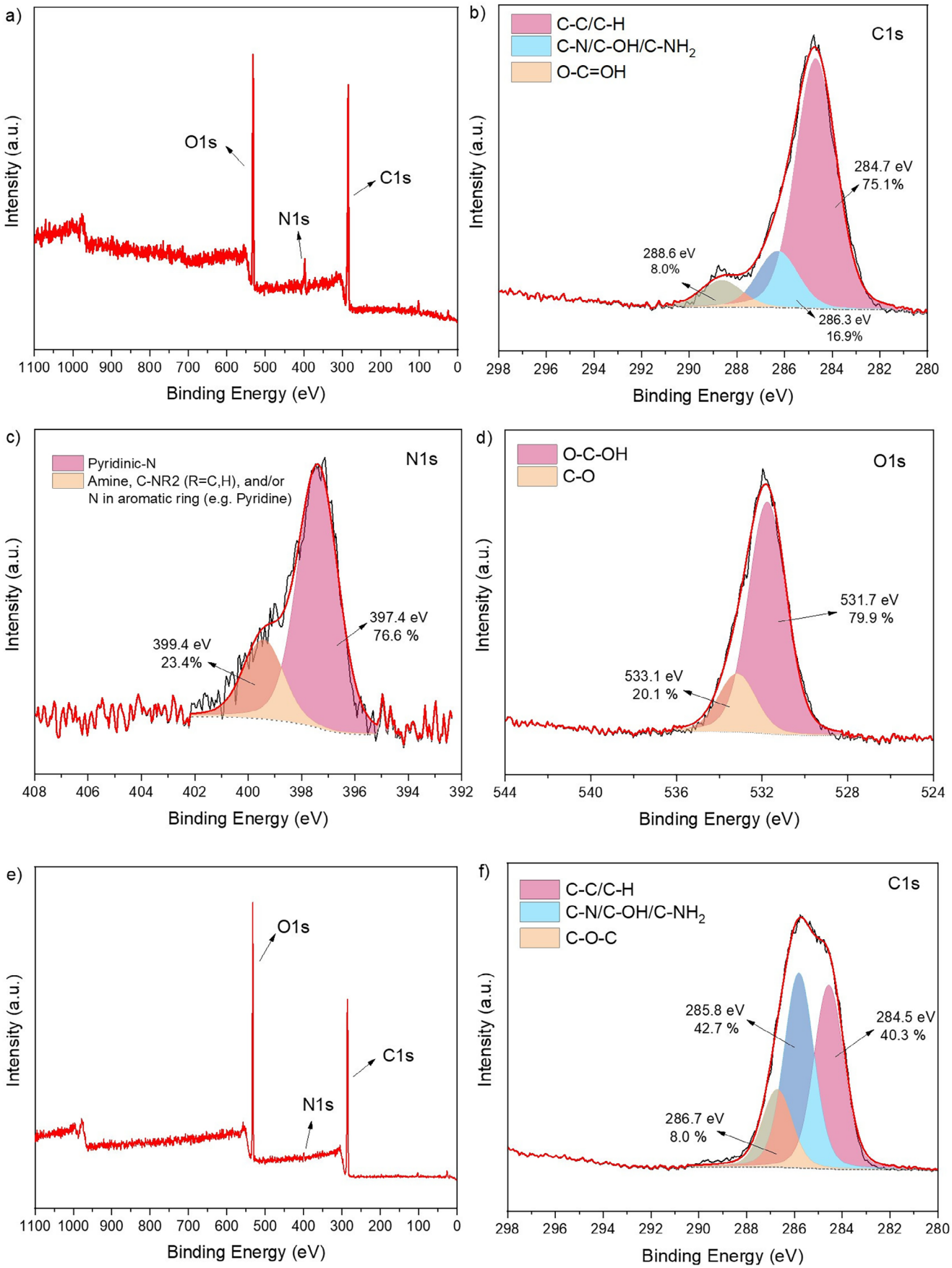

FIGURE 4 | XPS spectra of 50% CS/PVA before crosslinking, (a) survey spectrum, (b) C1s, (c) N1s, (d) O1s high-resolution spectra; and XPS spectra of 50% CS/PVA after crosslinking, (e) survey spectrum, (f) C1s, (g) N1s, (h) O1s high-resolution spectra and (i) cross-linked CS/PVA schematic representation. [Color figure can be viewed at wileyonlinelibrary.com]

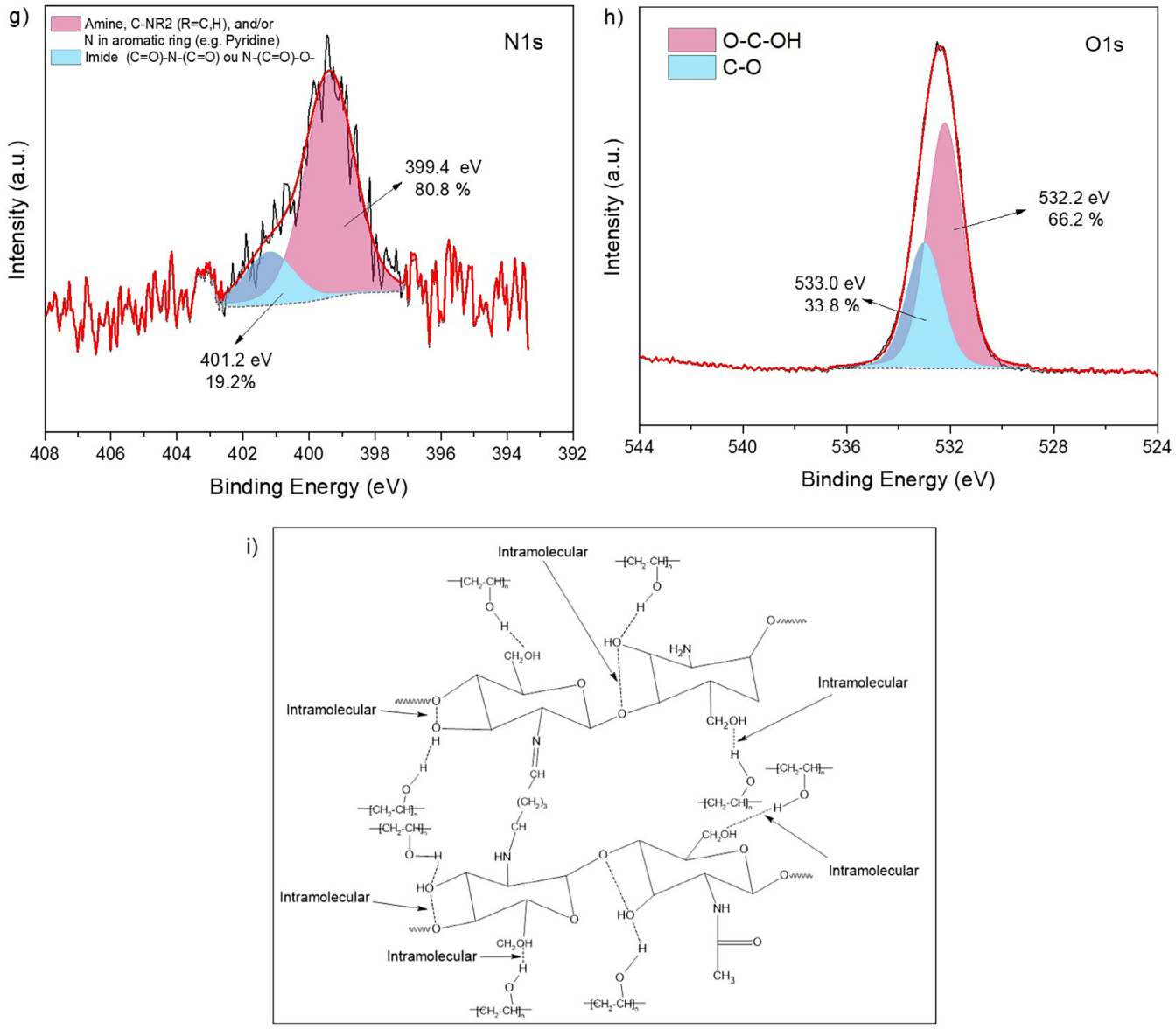

FIGURE 4 | (Continued)

with adjacent molecules or atoms [70, 71]. The literature reports that chitosan presents peaks at $2\theta = 10°$ and 20°, arising from inter- and intra-molecular hydrogen bonds through the presence of chitosan free amino groups [72–77]. In addition, chitosan has its spectrum in XRD corresponding to ICDD card No. [00-039-1894] with the main amorphous phase, and the peak at $2\theta = 20°$ was related to the presence of chitosan [78–80]. In the present study, peaks were observed at $2\theta = 10°$ and 19.9°.

The reduction in the semicrystalline nature of CS/PVA was indicated by the decrease in peak intensity and enlargement, or the overlap, suggesting the interaction between chitosan and PVA. According to the literature [47, 81, 82], if no such interaction occurs, there will be no alteration in the crystalline characteristics.

The influence of chitosan and glutaraldehyde on the stability of CS/PVA fibers was evaluated by thermogravimetric analysis (Figure 6). Pure PVA and pure chitosan present three stages of mass loss [30, 47, 83–85].

The initial mass loss (first stage) occurs below 100°C and is attributed to the release of hydrogen-bonded water [81]. The second stage results from the removal of the organic function —OH and the rupture of the polymeric chain, with the formation of polyene structures in PVA (190°C–294°C) [30, 83, 84]; and dehydration of saccharide rings, depolymerization, and decomposition in chitosan (270°C–320°C) [47]. An increase in the decomposition temperature of CS/PVA was observed upon the addition of chitosan, indicating greater thermal stability of the fibers, which can be attributed to the interaction between the polymers [82]. The interaction between the $—NH_2$ and —OH functional groups, originating from chitosan and PVA, resulting from the miscibility between the polymers, reduces the mobility of the polymer chains and increases thermal stability [41, 82]. The third event (370°C–470°C) is related to the decomposition of residual components formed by the previous stage [30, 83–86].

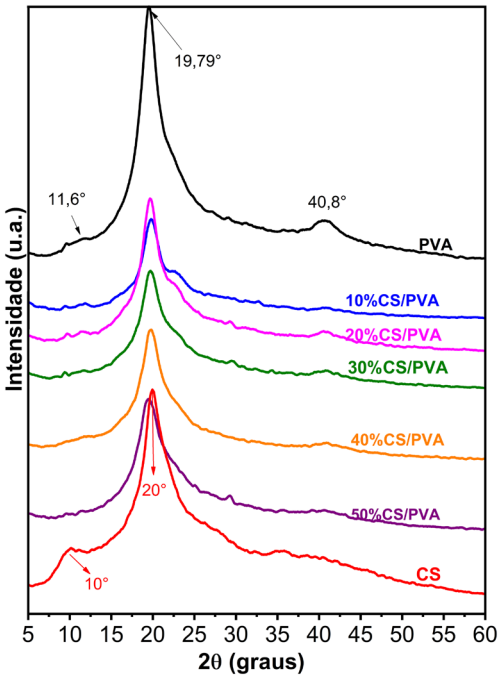

FIGURE 5 | X-ray diffractograms of CS/PVA and PVA fibers and CS powder. [Color figure can be viewed at wileyonlinelibrary.com]

Cross-linking with glutaraldehyde (Figure 6c,d) resulted in a new loss of mass during the first stage, with a peak near 130°C attributed to the release of acetic acid residues [87]. The cross-linked PVA fibers exhibited increased thermal stability during the second stage, which is due to the formation of acetal rings and ether bonds resulting from the reaction between the hydroxyl groups and glutaraldehyde [81]. However, the cross-linking process did not significantly affect the thermal stability of CS/PVA, as the mass loss profiles of the samples before and after cross-linking were similar.

The DSC thermograms of PVA and CS/PVA fibers, shown in Figure 7, provide a detailed and comprehensive visualization of the complex thermal transitions. There are polymers in which the glass transition temperature (T_g) is related to the relaxation of polymer chains [88–90]. Relaxation α is associated with the glass transition of the amorphous phase from intra- and intermolecular interactions [91]. Pure PVA exhibited a relaxation temperature of 94.3°C, whereas the relaxation temperatures for 10% CS/PVA, 20% CS/PVA, 30% CS/PVA, and 40% CS/PVA were 81.6°C, 82.4°C, 101.9°C, and 106.3°C, respectively. The corresponding relaxation enthalpy values are summarized in Table 1, with the 40% CS/PVA system having the highest value of 184.79 J/g, compared to 94.31 J/g for pure PVA and 120.51 J/g for the 10% CS/PVA system.

The change in the composition of the CS/PVA system altered the relaxation temperature, due to the increase in the chitosan concentration. Greater interactions are caused, transforming the mobility of the polymeric chains [92].

On the other hand, the amount of water influences the relaxation of CS chains. High humidity will provide additional relaxation in the chain, known as β_{moist} relaxation [88, 91]. As presented, TG (Figure 6) corroborates the presence of water in the CS/PVA system, demonstrating the decrease in sample weight during the heating scan.

Therefore, the humidity at which the fiber is formed will interfere with the relaxation of the polymer chain, and consequently, the relaxation temperature and the glass transition temperature of the material. It is also observed that after crosslinking, the relaxation temperature of the PVA and CS/PVA system increased, indicating chemical modification of the fibers.

The wettability of the CS/PVA composition after crosslinking with glutaraldehyde was evaluated through the contact angle, as shown in Figure 8. Chitosan and PVA are polar compositions due to the presence of —NH_2, —COOH, and —OH groups, respectively. A contact angle variation between $90° < \theta \leq 180°$ indicates an apolar character, whereas $\theta < 90°$ indicates a polar character, correlating with hydrophobic and hydrophilic properties, respectively [93–96]. Chitosan exhibits a contact angle of 98.3°, indicating a high hydrophobic character, whereas PVA has a contact angle of 52.4°, indicating the lowest hydrophobic character. A more hydrophobic character was expected with the increase in the chitosan concentration in CS/PVA [97] however, no statistically significant alterations were observed with the addition of CS in the PVA.

The apparent porosity and water uptake of the cross-linked 3D fibrous materials are presented in Figure 9a,b, respectively. The apparent porosity of the 3D fibrous material is important in terms of their association with their filtration capacity and permeability when used as membranes. As shown in Figure 7a, porosity greater than 92% for CS/PVA was achieved. This level of porosity is characteristic of aerogel materials and is desirable because it provides a significant surface area per unit volume of the membrane, thereby enhancing its effectiveness for liquid filtration applications [98]. The addition of chitosan to the fibers to form CS/PVA did not alter the apparent porosity of the 3D cotton-like structure. All samples were highly porous, which is very interesting for permeability and filtration processes [99].

The amount of CS influenced the water uptake behavior (Figure 9b). In this study, water uptake increased with the rise in CS content, suggesting an influence of interactions between the —OH and —NH_2 groups on the water uptake behavior [100]. However, at low concentrations of CS, a decrease in water uptake was observed compared to PVA. In general, the hydroxyl, amine, and ether functional groups present in the chitosan structure contribute with three electron pairs capable of forming hydrogen bonds with the five hydroxyl groups of PVA. If hydrogen bonding occurs between all the functional groups of both PVA and chitosan, a reduction in the availability of hydrophilic groups to interact with water absorption may take place [101]. This could explain the behavior observed in the 10% CS/PVA and 20% CS/PVA fibers.

PVA/CS films reported in the literature [102] had a maximum water uptake capacity of 298% ± 1%, with membrane saturation reached after 60 min of exposure to water. In addition. The literature suggests that a higher water absorption capacity is associated with a greater amount of PVA, compared

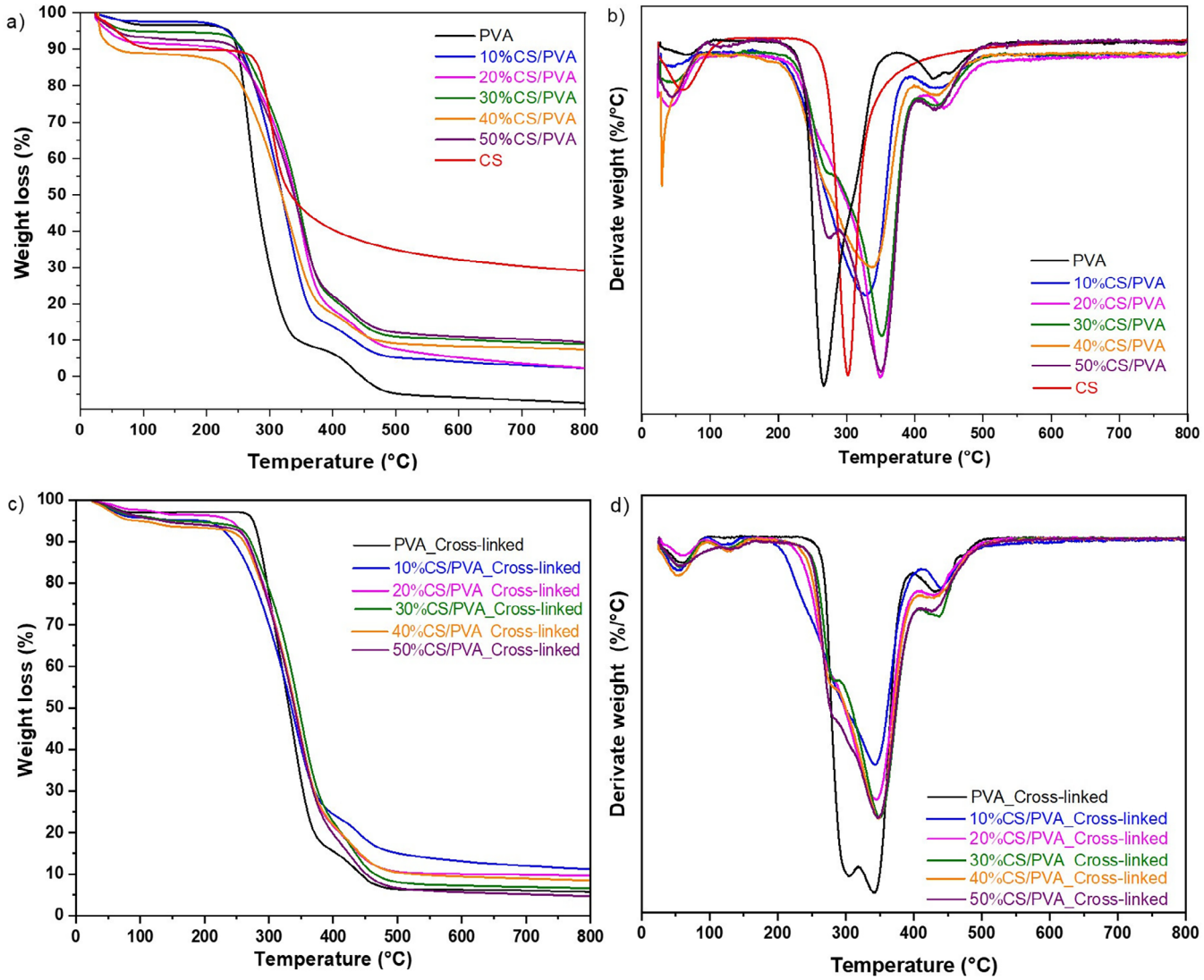

FIGURE 6 | TG (a) and DTG (b) thermographs of CS/PVA samples; and TG (c) and DTG (d) thermographs of the CS/PVA samples cross-linked with glutaraldehyde. [Color figure can be viewed at wileyonlinelibrary.com]

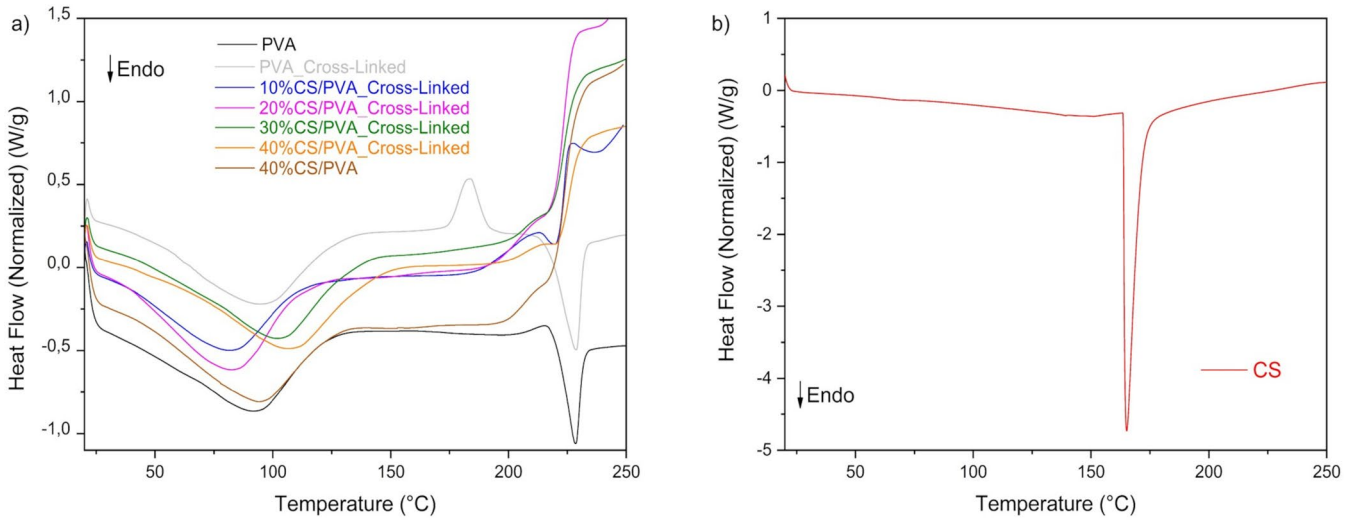

FIGURE 7 | DSC curves for (a) CS/PVA and PVA fibers and (b) CS powder. [Color figure can be viewed at wileyonlinelibrary.com]

TABLE 1 | Parameters obtained from the heat flow curves for CS/PVA and PVA fibers.

Composition	$T_{relaxation}$ (°C)	$\Delta H_{relaxation}$ (J/g)
PVA	91.7	145.18
PVA cross-linked	94.3	152.22
10% CS/PVA cross-linked	81.5	122.18
20% CS/PVA cross-linked	82.4	154.26
30% CS/PVA cross-linked	101.7	186.65
40% CS/PVA cross-linked	106.3	185.26
40% CS/PVA	93.7	146.06
CS	165.2	210.84

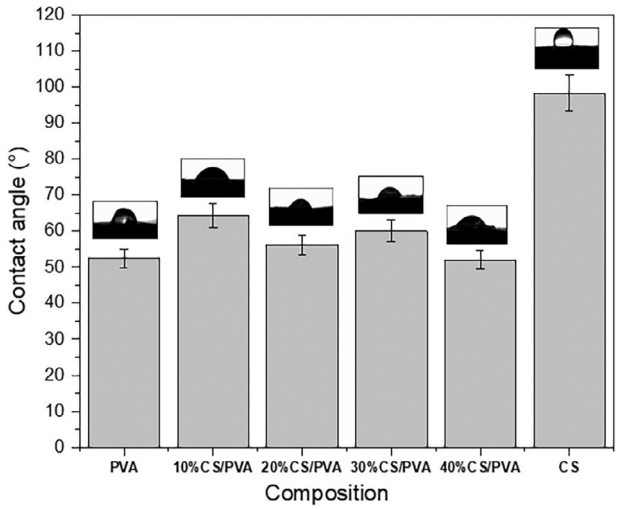

FIGURE 8 | Contact angle of the fibrous surface CS/PVA.

to chitosan, in studies involving low amounts of chitosan [42, 48, 103, 104]. Such behavior was attributed to the greater affinity of the hydroxyl group for water, resulting from the formation of hydrogen bonds. On the other hand, in this work, an increase in chitosan content can enhance water absorption capacity, when high amounts of chitosan is used (higher than 20%), likely because it provides a greater number of hydroxyl and amine groups that can interact with water molecules and form hydrogen bonds [105].

3.2 | Removal of *Microcystis aeruginosa*

Figure 10a–c shows the results of *Microcystis aeruginosa* removal, considering the turbidity parameter and Figure 8d–f is related to the Capture efficiency of *Microcystis aeruginosa* cells. Colonies of *Microcystis aeruginosa* containing 2.6×10^4–3.7×10^5 cells mL^{-1} were removed by CS/PVA nanofibrous cotton-wool-like materials, showing satisfactory results higher than 80% after 20 min of contact, depending on the concentration of chitosan and of nanofibers in the medium. The addition of chitosan to PVA altered the removal capacity of the fibers and increased the reduction capacity of turbidity (removal of cells) by up to 325%.

Park et al. [15], reports that cotton fibers modified with chitosan were able to remove up to 95.8% of *Microcystis aeruginosa* from a culture of $6.93\pm13\times10^5$ cells/mL after 12 h of treatment. In another study [106], biochar derived from algae sludge treated with 1.0 mol/L of HCl, to increase the efficiency, presented a turbidity removal of 90% after 12 h of treatment. In this study, the 10% and 20% CS/PVA achieved from 80% to 90% turbidity removal due to the capture of *Microcystis aeruginosa* cells after just 20 min of contact between the water and the fibers.

Moreover, studies [107] used cotton fibers modified with polyethyleneimine (PEI) *Microcystis aeruginosa* at concentrations ranging from 1% to 3% for the removal of *Microcystis aeruginosa*, achieving efficiencies of 65%–94% after 1 h. Thus, the developed material demonstrated high efficiency in removing *Microcystis*

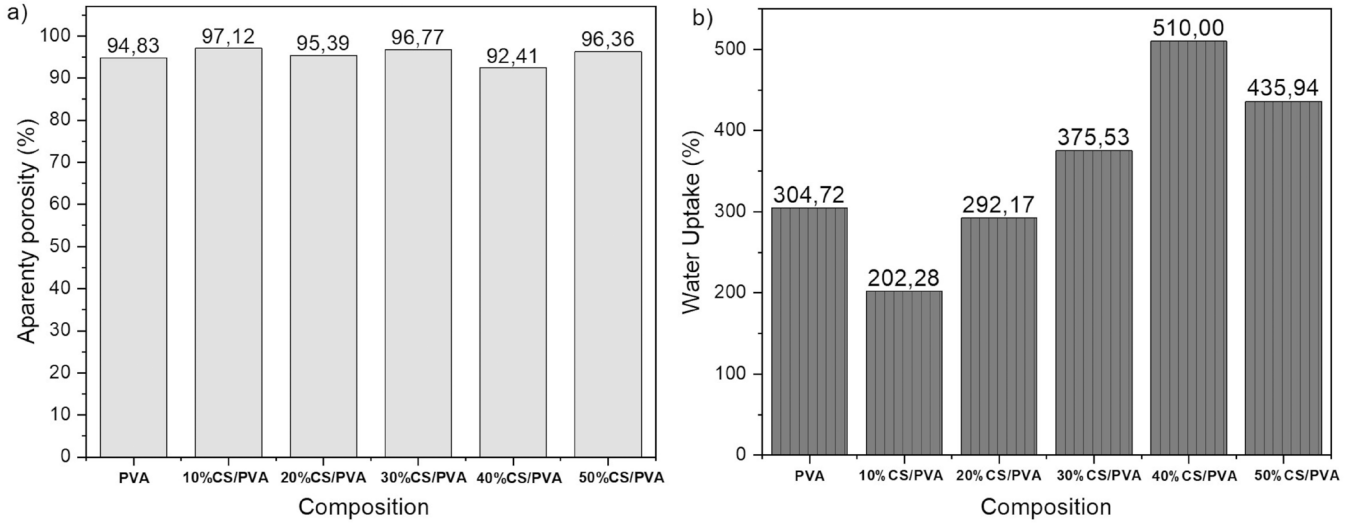

FIGURE 9 | (a) Apparent porosity and (b) water uptake for cross-linked CS/PVA fibers.

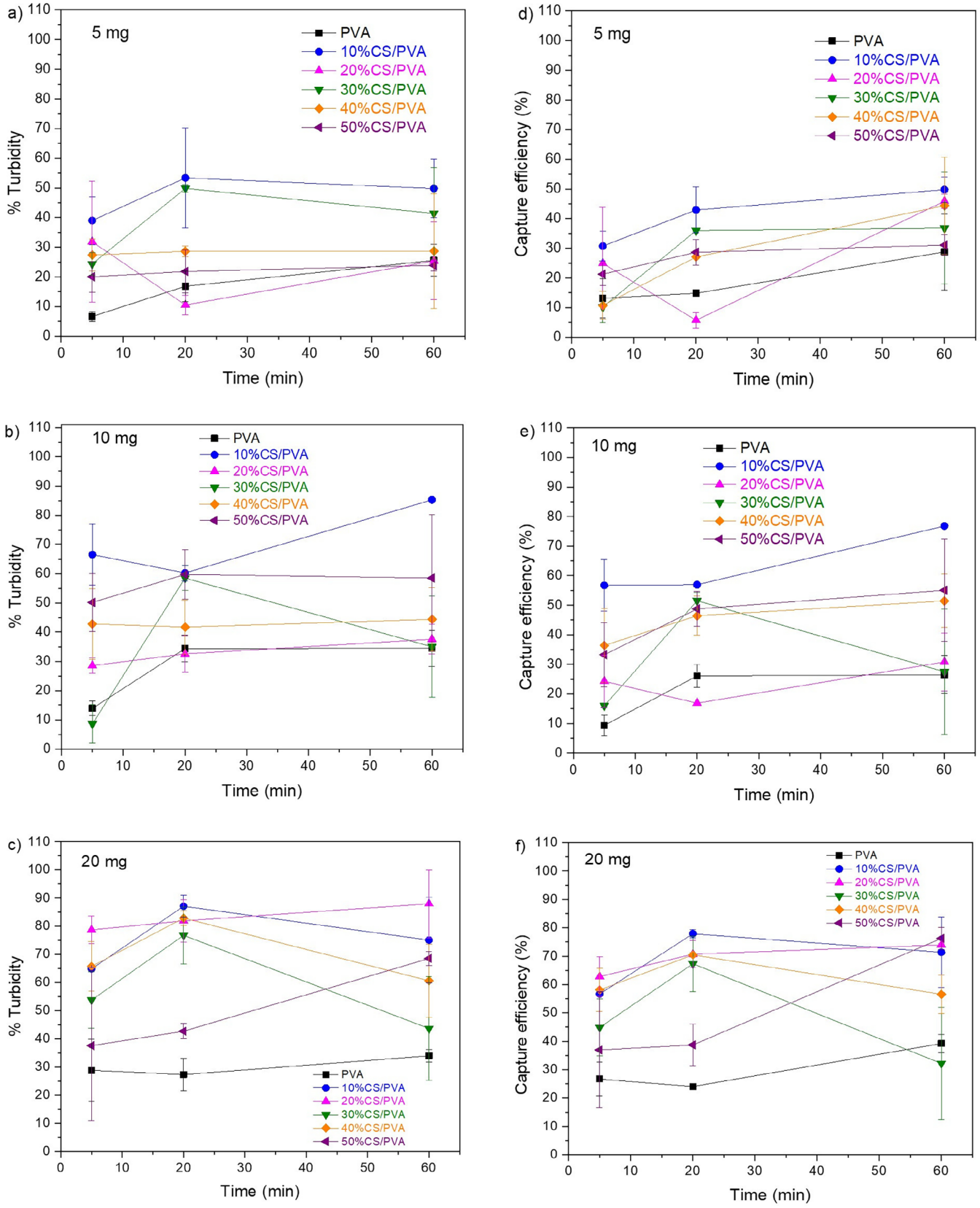

FIGURE 10 | Removal results through the analysis of turbidity (a–c) and capture efficiency (d–f), variation of removal time and the amount of CS/PVA (a, d) 5 mg; (b, e) 10 mg; (c, f) 20 mg. [Color figure can be viewed at wileyonlinelibrary.com]

aeruginosa compared to other fibrous materials, whereas also offering a fast process and an environmentally friendly approach using biodegradable materials.

As observed in Figure 10, the performance of cyanobacteria removal was related to the chitosan concentration in the fiber and the adsorbent concentration. Increasing the concentration of

the nanofiber adsorbent from 0.5 to 2.0 g L^{-1} decreases the time and increases the removal efficiency of *Microcystis aeruginosa*. The higher concentration of the adsorbent generates an increase in the number of active sites, allowing cyanobacteria to be adsorbed more effectively [108]. Chitosan nanofibers are positively charged adsorbents because of the protonated amine groups [14]. The removal of *Microcystis aeruginosa* was likely achieved through an adsorption mechanism. As reported, *Microcystis aeruginosa* has a negative surface charge due to the deprotonation of carboxyls and hydroxyl groups [15]. Providing the ability to be electrostatically adsorbed by cationic adsorbents.

The addition of 10% chitosan in PVA fibers increased adsorptive capacity by up to 325% for 20 mg of adsorbent. It was expected that the increase from 10% to 50% would provide greater adsorptive capacity. Since there would be greater electrostatic attraction between the $-NH_2$ groups (present in chitosan) and the cells of *Microcystis aeruginosa* [15].

Studies have reported that increasing the chitosan concentration enhances the removal of cyanobacteria [12, 23]. However, in these studies, chitosan was used as a coagulant for removing cyanobacteria. In another study, aimed at enhancing the number of amine groups on polyethyleneimine (PEI) and boosting its adsorption capacity, chitosan was used to produce PEI-modified chitosan-waste biomass composite fibers. These fibers were able to remove 91.2% of *Microcystis aeruginosa* [109] when modified with 1% w/w chitosan (degree of deacetylation, 75%–85%).

However, this direct relation between adsorption and CS content was not observed. It is possible that the balance between attractive and repulsive charges between the adsorbent and the adsorbate may have been disrupted due to the high amount of chitosan. To date, no studies have explored the use of high chitosan concentrations in fibrous systems, likely due to processing challenges associated with these high concentrations. This highlights the need for further research to better understand *Microcystis aeruginosa*.

The adsorption mechanism can be elucidated through the analysis of the zero charge potential (PCZ), which indicates the surface charge of the adsorbent material and the cyanobacteria, allowing one to infer the occurrence of attractive or repulsive electrostatic interactions between them. According to [12], chitosan-modified cellulose (CF) fiber exhibits an evident increase in positive charges, with the zeta potential changing from −3.1 mV to approximately 6.12 mV at pH 7. The zeta potentials of *Microcystis aeruginosa* are negative over a wide pH range [12, 110], at −30 mV at pH 7 [12].

The release of MC-LR cyanotoxin occurs through the cell lysis of *Microcystis aeruginosa*. Studies indicate that the adsorption process does not cause cell lysis [111]. In Figure 11, concentrations lower than 0.01 μg/L of MC-LR were detected after the removal of the cyanobacteria, indicating that cell lysis did not occur during treatment. Cellulose fibers modified with chitosan were able to reduce the concentration of MC-LR to 0.24 ± 0.04 μg/L after treatment. This reduction may be attributed to the adsorptive capacity of fibers in relation to cyanotoxins [18]. In addition, another study demonstrated that chitosan-modified cotton fibers also have the ability to reduce MC-LR concentration after treatment [15].

In cellulose fibers modified with chitosan and iron, the modifier containing $-NH_2$ is used to optimize the interactions of the adsorbent particles or fibers with the negatively charged algae. This description of the mechanism suggests a physical or electrostatic bond, characteristic of adsorption, rather than a process that would cause the rupture of the cell membrane. At the increased concentration of Fe^{3+}, 79% MC-LR was removed simultaneously. If cell lysis were the primary mechanism, an initial increase in the concentration of MC-LR in the water would be expected due to the release of the intracellular toxins, prior to any removal process.

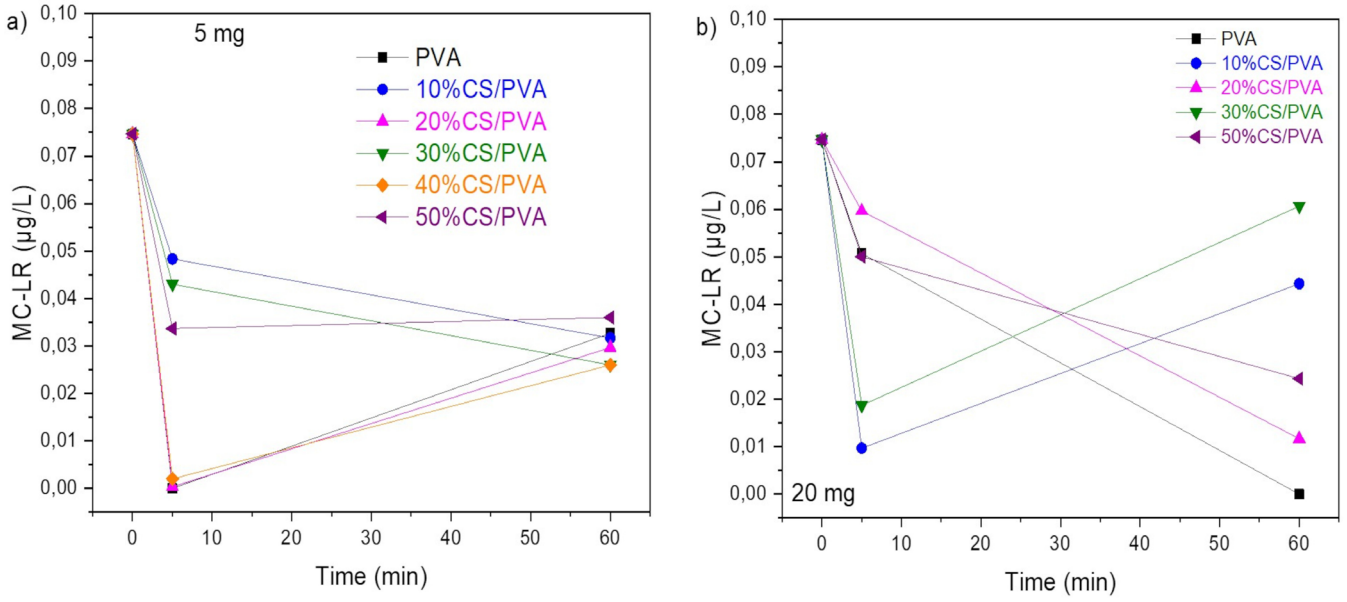

FIGURE 11 | MC-LR concentration after treatment of *Microcystis aeruginosa* with CS/PVA fibers. [Color figure can be viewed at wileyonlinelibrary.com]

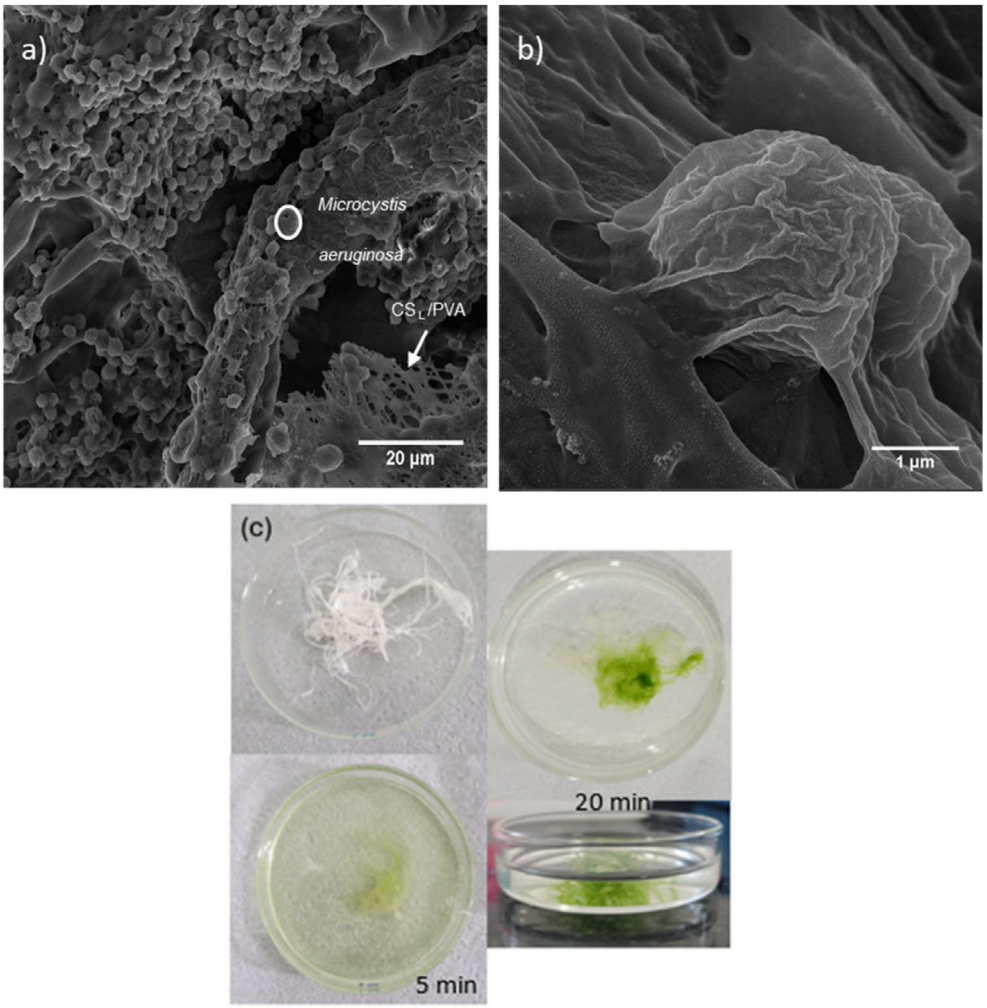

FIGURE 12 | FEG-SEM image of *Microcystis aeruginosa* capture in nanofibers at (a) 3 k× magnification; (b) 50 k×; and (c) Photograph of *Microcystis aeruginosa* in nanofibers (after 5 and 20 min of contact). [Color figure can be viewed at wileyonlinelibrary.com]

Simultaneous removal of algae and MC-LR suggests that the cells are removed intact or that the released MC-LR is immediately adsorbed, which still aligns with the adsorption mechanism [12].

According to the FEG-SEM images of the cyanobacteria shown in Figure 12a,b, the preservation of the spherical cell shape on the nanofibrous surface was observed, along with the presence of roughness. This indicates that no cell lysis occurred during the removal treatment [112]. The filaments around the cells are attributed to metabolites that can be released naturally [113]. The change in color of the nanofibers from white to green, Figure 12c, is related to the chlorophyll pigment present in *Microcystis aeruginosa*. Park et al. [18] observed that the removal of *Microcystis aeruginosa* using cotton fibers treated with chitosan resulted in a change in fiber color to green, which they attributed to the presence of chlorophyll from the cyanobacteria. Therefore, the green coloration can serve as a visual indicator of adsorption and interaction between the fibers and the bacteria.

It should be noted that the removal of cyanobacteria without releasing cyanotoxins due to cell damage is a safer removal process. When cell rupture occurs, the toxin released remains in an aqueous medium, presenting a greater capacity for pollution in the effluents. Thus, methods that are efficient in removing *Microcystis aeruginosa* without cell lysis are significantly important in drinking water treatment [17].

4 | Conclusions

The study demonstrated that CS/PVA nanofibers produced by the Air-Heated Solution Blow Spinning (A-HSBS) method are effective in removing *Microcystis aeruginosa* from contaminated water. The addition of 20 mg to fibers with 10% chitosan promoted the removal of cyanobacteria by up to 90% in just 20 min, compared to 30% for PVA fibers. The characterization of the fibers showed a highly porous 3D morphology, with fibers with diameters ranging from 230 ± 73 to 340 ± 102 nm, making them suitable for the adsorption process. Chitosan provided variations in thermal stability, hydrophilic character, and water uptake of the system. Thus, the developed fibers have great potential for applications in treating contaminated water, demonstrating high efficiency in the environmental remediation of pollutants. In comparison to previous studies, the present work achieved similar removal efficiencies (up to 90%) but in a significantly shorter contact time of just 20 min, using a simpler and scalable

fiber production method (A-HSBS) without requiring additional chemical modifiers. These results emphasize the superior removal kinetics and practical applicability of CS/PVA nanofibers for the rapid treatment of cyanobacteria-contaminated waters.

Author Contributions

Cynthia Ribeiro Guimarães: conceptualization (equal), formal analysis (equal), investigation (equal), methodology (equal), writing – original draft (equal), writing – review and editing (equal). **Valderi Duarte Leite:** methodology (supporting), resources (supporting). **Raquel Santos Leite:** conceptualization (supporting), investigation (supporting). **Maria Virgínia da Conceição Albuquerque:** investigation (supporting), methodology (supporting). **Ingridy Dayane dos Santos Silva:** investigation (supporting), methodology (equal), writing – original draft (supporting). **Renate Maria Ramos Wellen:** methodology (supporting). **Gelmires de Araújo Neves:** funding acquisition (equal), resources (equal), writing – review and editing (supporting). **Valmor Roberto Mastelaro:** formal analysis (supporting), investigation (supporting), methodology (supporting), writing – review and editing (supporting). **Romualdo Rodrigues Menezes:** investigation (lead), methodology (lead), resources (lead), supervision (lead), writing – original draft (lead), writing – review and editing (lead).

Acknowledgments

The authors would like to thank CNPq (grant Nos. 141518/2021-9, 420004/2018-1, 309771/2021-8 and309234/2020-4), FAPESQ (Grant term nº3064/2021 and grant term nº 036/2023/PRONEX) and FAPESP (Grant number 2013/07296-2) for financial support. We would like to express our gratitude to the Transmission Electron Microscopy Laboratory (LabMET/UFAL) for conducting the TEM analyses. The Article Processing Charge for the publication of this research was funded by the Coordenação de Aperfeiçoamento de Pessoal de Nível Superior - Brasil (CAPES) (ROR identifier: 00x0ma614).

Data Availability Statement

The data that support the findings of this study are available from the corresponding author upon reasonable request.

References

1. S. Zhang, Y. Chen, X. Zang, and X. Zhang, "Harvesting of *Microcystis aeruginosa* Using Membrane Filtration: Influence of Pore Structure on Fouling Kinetics, Algogenic Organic Matter Retention and Cake Formation," *Algal Research* 52 (2020): 102112, https://doi.org/10.1016/j.algal.2020.102112.

2. H. Liu, S. Chen, H. Zhang, et al., "Effects of Copper Sulfate Algaecide on the Cell Growth, Physiological Characteristics, the Metabolic Activity of *Microcystis aeruginosa* and Raw Water Application," *Journal of Hazardous Materials* 445 (2023): 130604, https://doi.org/10.1016/j.jhazmat.2022.130604.

3. Q. N. Tran, X. Jin, and N. Q. H. Doan, "Enhanced Removal of Extracellular Microcystin-LR Using Chitosan Coagulation-Ultrafiltration: Performance and Mechanism," *Journal of Environmental Chemical Engineering* 10 (2022): 107902, https://doi.org/10.1016/j.jece.2022.107902.

4. X. He, Y. L. Liu, A. Conklin, et al., "Toxic Cyanobacteria and Drinking Water: Impacts, Detection, and Treatment," *Harmful Algae* 54 (2016): 174–193, https://doi.org/10.1016/j.hal.2016.01.001.

5. M. G. Hinojosa, D. Gutiérrez-Praena, A. I. Prieto, R. Guzmán-Guillén, A. Jos, and A. M. Cameán, "Neurotoxicity Induced by Microcystins and Cylindrospermopsin: A Review," *Science of the Total Environment* 668 (2019): 547–565, https://doi.org/10.1016/j.scitotenv.2019.02.426.

6. I. Gardi, Y. G. Mishael, M. Lindahl, A. M. Muro-Pastor, and T. Undabeytia, "Coagulation-Flocculation of *Microcystis aeruginosa* by Polymer-Clay Based Composites," *Journal of Cleaner Production* 394 (2023): 136356, https://doi.org/10.1016/j.jclepro.2023.136356.

7. J. Marumure, W. Gwenzi, Z. Makuvara, et al., "Global Occurrence of Cyanotoxins in Drinking Water Systems: Recent Advances, Human Health Risks, Mitigation, and Future Directions," *Lifestyles* 15 (2025): 825, https://doi.org/10.3390/life15050825.

8. S. H. Premathilaka, J. A. Westrick, and D. Isailovic, "Discovery of Novel Hydroxyproline-Containing Microcystins in Western Lake Erie Cyanobacterial Bloom Samples," *ACS ES&T Water* 5 (2025): 2352–2360, https://doi.org/10.1021/acsestwater.4c01241.

9. S. Ghaju, E. Pakuwal, R. S. C. Takeshita, X. Mou, and W. C. J. Chung, "Short-Term Ingestion of Sublethal Microcystin Levels Disrupts Stress Response in Male Mice," *Frontiers in Endocrinology* 16 (2025): 1568923, https://doi.org/10.3389/fendo.2025.1568923.

10. Q. Zhai, L. Song, X. Ji, et al., "Research Progress of Advanced Oxidation Technology for the Removal of *Microcystis aeruginosa*: A Review," *Environmental Science and Pollution Research* 29 (2022): 40449–40461, https://doi.org/10.1007/s11356-022-19792-w.

11. M. P. Doers and D. L. Parker, "Properties of *Microcystis aeruginosa* and *M. flos-aquae* (cyanophyta) in Culture: Taxonomic Implications," *Journal of Phycology* 24 (1988): 502–508.

12. M. Liu, J. Zhang, L. Wang, H. Zhang, W. Zhang, and X. Zhang, "Removal of *Microcystis aeruginosa* and Microcystin-LR Using Chitosan (CTS)-Modified Cellulose Fibers and Ferric Chloride," *Separation and Purification Technology* 308 (2023): 122889, https://doi.org/10.1016/J.SEPPUR.2022.122889.

13. S. Sun, Q. Tang, H. Xu, et al., "A Comprehensive Review on the Photocatalytic Inactivation of *Microcystis aeruginosa*: Performance, Development, and Mechanisms," *Chemosphere* 312 (2023): 137239, https://doi.org/10.1016/J.CHEMOSPHERE.2022.137239.

14. G. Nam, M. M. Mohamed, and J. Jung, "Novel Treatment of *Microcystis aeruginosa* Using Chitosan-Modified Nanobubbles," *Environmental Pollution* 292 (2022): 118458, https://doi.org/10.1016/J.ENVPOL.2021.118458.

15. Y. H. Park, S. Kim, J. S. Choi, J. Chung, J. S. Choi, and Y. E. Choi, "Chitosan-Modified Cotton Fiber: An Efficient and Reusable Adsorbent in Removal of Harmful Cyanobacteria, *Microcystis aeruginosa* From Aqueous Phases," *Chemosphere* 349 (2024): 140679, https://doi.org/10.1016/J.CHEMOSPHERE.2023.140679.

16. M. Mucci, I. A. Guedes, E. J. Faassen, and M. Lürling, "Chitosan as a Coagulant to Remove Cyanobacteria Can Cause Microcystin Release," *Toxins* 12 (2020): 711, https://doi.org/10.3390/toxins12110711.

17. T. E. Grigoriev, K. I. Lukanina, P. M. Gotovtsev, et al., "Chitosan-Based Fiber-Sponge Materials as a Promising Tool for Microalgae Harvesting From Lake Baikal," *Journal of Applied Polymer Science* 137 (2020): 49209, https://doi.org/10.1002/app.49209.

18. Y. H. Park, S. Kim, H. S. Kim, C. Park, and Y. E. Choi, "Adsorption Strategy for Removal of Harmful Cyanobacterial Species *Microcystis aeruginosa* Using Chitosan Fiber," *Sustainability* 12 (2020): 4587, https://doi.org/10.3390/su12114587.

19. G. A. V. Magalhães-Ghiotto, J. P. S. Natal, M. R. Guilherme, R. G. Gomes, and R. Bergamasco, "Evaluation of the Removal of Cyanobacteria and Cyanotoxins With a Composite Hydrogel Based on Chemically Modified Gelatin and PVA-Containing Graphene Oxide Nanoparticles," *Environmental Nanotechnology, Monitoring & Management* 22 (2024): 100995, https://doi.org/10.1016/J.ENMM.2024.100995.

20. Y. Mei, S. Runjun, F. Yan, W. Honghong, D. Hao, and L. Chengkun, "Preparation, Characterization and Kinetics Study of Chitosan/PVA Electrospun Nanofiber Membranes for the Adsorption of Dye From

Water," *Journal of Polymer Engineering* 39 (2019): 459–471, https://doi.org/10.1515/polyeng-2018-0275.

21. S. Rezaei Soulegani, Z. Sherafat, and M. Rasouli, "Morphology, Physical, and Mechanical Properties of Potentially Applicable Coelectrospun Polysulfone/Chitosan-Polyvinyl Alcohol Fibrous Membranes in Water Purification," *Journal of Applied Polymer Science* 138 (2021): 49933, https://doi.org/10.1002/app.49933.

22. M. R. Karim, M. O. Aijaz, N. H. Alharth, H. F. Alharbi, F. S. Al-Mubaddel, and M. R. Awual, "Composite Nanofibers Membranes of Poly(Vinyl Alcohol)/Chitosan for Selective Lead(II) and Cadmium(II) Ions Removal From Wastewater," *Ecotoxicology and Environmental Safety* 169 (2019): 479–486, https://doi.org/10.1016/j.ecoenv.2018.11.049.

23. H. Y. Pei, C. X. Ma, W. R. Hu, and F. Sun, "The Behaviors of *Microcystis aeruginosa* Cells and Extracellular Microcystins During Chitosan Flocculation and Flocs Storage Processes," *Bioresource Technology* 151 (2014): 314–322, https://doi.org/10.1016/j.biortech.2013.10.077.

24. C. F. Mok, Y. C. Ching, F. Muhamad, N. A. Abu Osman, N. D. Hai, and C. R. Che Hassan, "Adsorption of Dyes Using Poly(Vinyl Alcohol) (PVA) and PVA-Based Polymer Composite Adsorbents: A Review," *Journal of Polymers and the Environment* 28 (2020): 775–793, https://doi.org/10.1007/s10924-020-01656-4.

25. O. Duman, H. Uğurlu, C. Ö. Diker, and S. Tunç, "Fabrication of Highly Hydrophobic or Superhydrophobic Electrospun PVA and Agar/PVA Membrane Materials for Efficient and Selective Oil/Water Separation," *Journal of Environmental Chemical Engineering* 10 (2022): 107405.

26. H. Lyu, Y. Han, R. Zhang, Y. Wu, and X. Wu, "Anti-Biofouling Multi-Modified Chitosan/Polyvinylalcohol Air-Blown Nanofibers for Selective Radionuclide Capture in Wastewater," *Separation and Purification Technology* 303 (2022): 122196, https://doi.org/10.1016/j.seppur.2022.122196.

27. R. de Sousa Victor, A. Marcelo da Cunha Santos, and B. Viana de Sousa, "A Review on Chitosan's Uses as Biomaterial: Tissue Engineering, Drug Delivery Systems and Cancer Treatment," *Materials* 13 (2020): 4995, https://doi.org/10.3390/ma13214995.

28. Z. Wang, F. Yan, H. Pei, J. Li, Z. Cui, and B. He, "Antibacterial and Environmentally Friendly Chitosan/Polyvinyl Alcohol Blend Membranes for Air Filtration," *Carbohydrate Polymers* 198 (2018): 241–248, https://doi.org/10.1016/j.carbpol.2018.06.090.

29. U. Duru Kamaci and A. Peksel, "Fabrication of PVA-Chitosan-Based Nanofibers for Phytase Immobilization to Enhance Enzymatic Activity," *International Journal of Biological Macromolecules* 164 (2020): 3315–3322, https://doi.org/10.1016/j.ijbiomac.2020.08.226.

30. B. Yang, J. Wang, L. Kang, X. Gao, and K. Zhao, "Antibacterial, Efficient and Sustainable CS/PVA/GA Electrospun Nanofiber Membrane for Air Filtration," *Materials Research Express* 9 (2022): 125002, https://doi.org/10.1088/2053-1591/aca74a.

31. G. Sargazi, D. Afzali, A. Mostafavi, and S. Y. Ebrahimipour, "Synthesis of CS/PVA Biodegradable Composite Nanofibers as a Microporous Material With Well Controllable Procedure Through Electrospinning," *Journal of Polymers and the Environment* 26 (2018): 1804–1817, https://doi.org/10.1007/s10924-017-1080-8.

32. B. Zhang, Z. Jiang, X. Li, et al., "Facile Preparation of Biocompatible and Antibacterial Water-Soluble Films Using Polyvinyl Alcohol/Carboxymethyl Chitosan Blend Fibers via Centrifugal Spinning," *Carbohydrate Polymers* 317 (2023): 121062, https://doi.org/10.1016/J.CARBPOL.2023.121062.

33. R. Liu, X. Xu, X. Zhuang, and B. Cheng, "Solution Blowing of Chitosan/PVA Hydrogel Nanofiber Mats," *Carbohydrate Polymers* 101 (2014): 1116–1121, https://doi.org/10.1016/J.CARBPOL.2013.10.056.

34. E. S. Medeiros, G. M. Glenn, A. P. Klamczynski, W. J. Orts, and L. H. C. Mattoso, "Solution Blow Spinning: A New Method to Produce Micro- and Nanofibers From Polymer Solutions," *Journal of Applied Polymer Science* 113 (2009): 2322–2330, https://doi.org/10.1002/app.30275.

35. V. C. Silva, R. M. C. Farias, R. F. Bonan, et al., "Novel Synthesis of BCP Cotton-Wool-Like Nanofibrous Scaffolds by Air-Heated Solution Blow Spinning (A-HSBS) Technique," *Ceramics International* 49 (2023): 24084–24092, https://doi.org/10.1016/J.CERAMINT.2023.04.241.

36. R. M. Oliveira Filho, R. F. Alves, R. A. Raimundo, et al., "Structural, Magnetic and Electrocatalytic Properties of Rock Salt Oxide Nanofibers (Ni0. 2Mg0. 2Zn0. 2Cu0. 2-xCo0. 2+x)O Produced by Air-Heated Solution Blow Spinning (A-HSBS) for Oxygen Evolution Reaction," *Applied Surface Science* 682 (2025): 161593, https://doi.org/10.1016/J.APSUSC.2024.161593.

37. R. N. de Araujo, R. A. Raimundo, G. d. A. Neves, et al., "α-Mn2O3 Porous Fibers Synthesized by Air-Heated Solution Blow Spinning (A-HSBS) Technique: Electrochemical Assessment for Oxygen Evolution Reaction in Alkaline Medium," *Journal of Physics and Chemistry of Solids* 192 (2024): 112086, https://doi.org/10.1016/J.JPCS.2024.112086.

38. K. C. Costa, M. G. d. S. Andrade, R. N. de Araujo, et al., "PVP as an Oxygen Vacancy-Inducing Agent in the Development of Black 45S5 Bioactive Glass Fibrous Scaffolds Doped With Zn and Mg Using A-HSBS," *Materials* 18 (2025): 1340, https://doi.org/10.3390/ma18061340.

39. L. N. L. C. Barros, V. C. Silva, R. N. de Araujo, D. B. Silva, G. d. A. Neves, and R. R. Menezes, "Production of 3D Fibrous Structure of ICIE16 Bioactive Glass by Air-Heated Solution Blow Spinning (A-HSBS)," *Materials Letters* 365 (2024): 136440, https://doi.org/10.1016/J.MATLET.2024.136440.

40. J. Cui, X. Niu, D. Zhang, et al., "The Novel Chitosan-Amphoteric Starch Dual Flocculants for Enhanced Removal of *Microcystis aeruginosa* and Algal Organic Matter," *Carbohydrate Polymers* 304 (2023): 120474, https://doi.org/10.1016/j.carbpol.2022.120474.

41. G. R. C. Cerqueira, D. S. Gomes, R. S. Victor, et al., "Development of PVA/Chitosan Nanofibers by a Green Route Using Solution Blow Spinning," *Journal of Polymers and the Environment* 32 (2023): 1489–1499, https://doi.org/10.1007/s10924-023-03033-3.

42. H. Adeli, M. T. Khorasani, and M. Parvazinia, "Wound Dressing Based on Electrospun PVA/Chitosan/Starch Nanofibrous Mats: Fabrication, Antibacterial and Cytocompatibility Evaluation and In Vitro Healing Assay," *International Journal of Biological Macromolecules* 122 (2019): 238–254, https://doi.org/10.1016/J.IJBIOMAC.2018.10.115.

43. R. A. Rebia, S. Rozet, Y. Tamada, and T. Tanaka, "Biodegradable PHBH/PVA Blend Nanofibers: Fabrication, Characterization, In Vitro Degradation, and In Vitro Biocompatibility," *Polymer Degradation and Stability* 154 (2018): 124–136, https://doi.org/10.1016/J.POLYMDEGRADSTAB.2018.05.018.

44. G. Wang, J. Kang, S. Yang, M. Lu, and H. Wei, "Influence of Structure Construction on Water Uptake, Swelling, and Oxidation Stability of Proton Exchange Membranes," *International Journal of Hydrogen Energy* 50 (2024): 279–311, https://doi.org/10.1016/j.ijhydene.2023.08.129.

45. M. V. d. C. Albuquerque, E. K. F. de Carvalho, C. A. P. de Lima, J. T. de Sousa, V. D. Leite, and W. S. Lopes, "Removal of Microcystin-LR From Eutrophic Water Using Solar Distillation," *Desalination and Water Treatment* 253 (2022): 138–144, https://doi.org/10.5004/dwt.2022.28286.

46. H. Utermöhl, "Zur Vervollkommnung Der Quantitativen Phytoplankton-Methodik," *SIL Communications* 9 (1958): 1–38, https://doi.org/10.1080/05384680.1958.11904091.

47. S. Biranje, P. Madiwale, and R. V. Adivarekar, "Electrospinning of Chitosan/PVA Nanofibrous Membrane at Ultralow Solvent Concentration," *Journal of Polymer Research* 24 (2017): 92, https://doi.org/10.1007/s10965-017-1238-z.

48. Y. Zhang, X. Huang, B. Duan, L. Wu, S. Li, and X. Yuan, "Preparation of Electrospun Chitosan/Poly(Vinyl Alcohol) Membranes," *Colloid & Polymer Science* 285 (2007): 855–863, https://doi.org/10.1007/s00396-006-1630-4.

49. S. Adibzadeh, S. Bazgir, and A. A. Katbab, "Fabrication and Characterization of Chitosan/Poly(Vinyl Alcohol) Electrospun Nanofibrous Membranes Containing Silver Nanoparticles for Antibacterial Water Filtration," *Iranian Polymer Journal* 23 (2014): 645–654, https://doi.org/10.1007/s13726-014-0258-3.

50. G. C. da Mata, M. S. Morais, W. P. de Oliveira, and M. L. Aguiar, "Composition Effects on the Morphology of PVA/Chitosan Electrospun Nanofibers," *Polymers* 14 (2022): 4856, https://doi.org/10.3390/polym14224856.

51. N. M. Mahmoodi and Z. Mokhtari-Shourijeh, "Preparation of PVA-Chitosan Blend Nanofiber and Its Dye Removal Ability From Colored Wastewater," *Fibers and Polymers* 16 (2015): 1861–1869, https://doi.org/10.1007/s12221-015-5371-1.

52. H. Hosseini, M. K. Shahraky, A. Amani, and F. S. Landi, "Electrospinning of Polyvinyl Alcohol/Chitosan/Hyaluronic Acid Nanofiber Containing Growth Hormone and Its Release Investigations," *Polymers for Advanced Technologies* 32 (2021): 574–581, https://doi.org/10.1002/pat.5111.

53. N. Rosli, W. Z. N. Yahya, and M. D. H. Wirzal, "Crosslinked Chitosan/Poly(Vinyl Alcohol) Nanofibers Functionalized by Ionic Liquid for Heavy Metal Ions Removal," *International Journal of Biological Macromolecules* 195 (2022): 132–141, https://doi.org/10.1016/j.ijbiomac.2021.12.008.

54. S. Wang, F. Yan, P. Ren, et al., "Incorporation of Metal-Organic Frameworks Into Electrospun Chitosan/Poly (Vinyl Alcohol) Nanofibrous Membrane With Enhanced Antibacterial Activity for Wound Dressing Application," *International Journal of Biological Macromolecules* 158 (2020): 9–17, https://doi.org/10.1016/j.ijbiomac.2020.04.116.

55. H. S. Mansur, E. de S. Costa, Jr., A. A. P. Mansur, and E. F. Barbosa-Stancioli, "Cytocompatibility Evaluation in Cell-Culture Systems of Chemically Crosslinked Chitosan/PVA Hydrogels," *Materials Science and Engineering: C* 29 (2009): 1574–1583, https://doi.org/10.1016/J.MSEC.2008.12.012.

56. T. H. N. Vu, S. N. Morozkina, and M. V. Uspenskaya, "Study of the Nanofibers Fabrication Conditions From the Mixture of Poly(Vinyl Alcohol) and Chitosan by Electrospinning Method," *Polymers* 14 (2022): 811, https://doi.org/10.3390/polym14040811.

57. M. Huang, J. Li, J. Chen, M. Zhou, and J. He, "Preparation of CS/PVA Nanofibrous Membrane With Tunable Mechanical Properties for Tympanic Member Repair," *Macromolecular Research* 26 (2018): 892–899, https://doi.org/10.1007/s13233-018-6127-8.

58. X. Wang, W. Deng, Y. Xie, and C. Wang, "Selective Removal of Mercury Ions Using a Chitosan–Poly(Vinyl Alcohol) Hydrogel Adsorbent With Three-Dimensional Network Structure," *Chemical Engineering Journal* 228 (2013): 232–242, https://doi.org/10.1016/J.CEJ.2013.04.104.

59. T. Lou, X. Yan, and X. Wang, "Chitosan Coated Polyacrylonitrile Nanofibrous Mat for Dye Adsorption," *International Journal of Biological Macromolecules* 135 (2019): 919–925, https://doi.org/10.1016/J.IJBIOMAC.2019.06.008.

60. B. S. de Farias, T. R. S. C. Junior, and L. A. d. A. Pinto, "Chitosan-Functionalized Nanofibers: A Comprehensive Review on Challenges and Prospects for Food Applications," *International Journal of Biological Macromolecules* 123 (2019): 210–220, https://doi.org/10.1016/j.ijbiomac.2018.11.042.

61. L. L. Min, Z. H. Yuan, L. b. Zhong, Q. Liu, R. X. Wu, and Y. M. Zheng, "Preparation of Chitosan Based Electrospun Nanofiber Membrane and Its Adsorptive Removal of Arsenate From Aqueous Solution," *Chemical Engineering Journal* 267 (2015): 132–141, https://doi.org/10.1016/J.CEJ.2014.12.024.

62. Y. Li, Y. Dai, Q. Tao, and L. Xu, "Synthesis and Characterization of Amino Acid-Functionalized Chitosan/Poly(Vinyl Alcohol) for Effective Adsorption of Uranium," *Journal of Radioanalytical and Nuclear Chemistry* 331 (2022): 4753–4765, https://doi.org/10.1007/s10967-022-08587-5.

63. Y. Wu, J. Zhang, S. Hu, Y. Zhang, J. Chan, and X. Xin, "Synthesis and Low Concentration Cr(Vi) Adsorption Performance of Chitosan/Poly(Vinyl Alcohol)/Fe(iii)/Glutaraldehyde," *Desalination and Water Treatment* 167 (2019): 291–301, https://doi.org/10.5004/dwt.2019.24648.

64. J. Hizal, N. Kanmaz, and M. Yılmazoğlu, "Evaluation of Humic Acid Embedded Chitosan/PVA Composite Performance in the Removal of Uranyl Ions," *Materials Chemistry and Physics* 299 (2023): 127483, https://doi.org/10.1016/J.MATCHEMPHYS.2023.127483.

65. Y. Li, J. Zhang, C. Xu, and Y. Zhou, "Crosslinked Chitosan Nanofiber Mats Fabricated by One-Step Electrospinning and Ion-Imprinting Methods for Metal Ions Adsorption," *Science China Chemistry* 59 (2016): 95–105, https://doi.org/10.1007/s11426-015-5526-3.

66. R. S. Juang, C. A. Liu, and C. C. Fu, "Polyaminated Electrospun Chitosan Fibrous Membranes for Highly Selective Removal of Anionic Organics From Aqueous Solutions in Continuous Operation," *Separation and Purification Technology* 319 (2023): 124043, https://doi.org/10.1016/J.SEPPUR.2023.124043.

67. F. M. Ali and F. Maiz, "Structural, Optical and AFM Characterization of PVA:La3+ Polymer Films," *Physica B: Condensed Matter* 530 (2018): 19–23, https://doi.org/10.1016/J.PHYSB.2017.10.124.

68. M. A. Morsi, A. H. Oraby, A. G. Elshahawy, and R. M. Abd El-Hady, "Preparation, Structural Analysis, Morphological Investigation and Electrical Properties of Gold Nanoparticles Filled Polyvinyl Alcohol/Carboxymethyl Cellulose Blend," *Journal of Materials Research and Technology* 8 (2019): 5996–6010, https://doi.org/10.1016/j.jmrt.2019.09.074.

69. H. Abral, J. Ariksa, M. Mahardika, et al., "Highly Transparent and Antimicrobial PVA Based Bionanocomposites Reinforced by Ginger Nanofiber," *Polymer Testing* 81 (2020): 106186, https://doi.org/10.1016/J.POLYMERTESTING.2019.106186.

70. M. M. H. Sachchu, F. K. Anik, S. Ahmed, et al., "Crystallographic Investigation of PVA@PLA Nanocomposite Film by X-Ray Diffraction: Insight From High Resolution TEM," *Journal of Engineering Research and Reports* 27 (2025): 310–327, https://doi.org/10.9734/jerr/2025/v27i31436.

71. A. Saeed and J. A. M. Abdulwahed, "Development and Characterization of PVA-Based Nanocomposites With Graphene and Natural Quartz Nanoparticles for Energy Storage Applications," *Journal of Energy Storage* 98 (2024): 113138, https://doi.org/10.1016/J.EST.2024.113138.

72. T. F. Jiao, J. Zhou, J. X. Zhou, L. H. Gao, Y. Xing, and X. Li, "Synthesis and Characterization of Chitosan-Based Schiff Base Compounds With Aromatic Substituent Groups," *Iranian Polymer Journal* 20 (2011): 123–136.

73. D. Arif, M. B. K. Niazi, N. Ul-Haq, M. N. Anwar, and E. Hashmi, "Preparation of Antibacterial Cotton Fabric Using Chitosan-Silver Nanoparticles," *Fibers and Polymers* 16 (2015): 1519–1526, https://doi.org/10.1007/s12221-015-5245-6.

74. J. Cao, H. Zhao, Z. Dong, and Z. Yang, "Allelopathic Effect of Chitosan Fiber on the Growth of *Microcystis aeruginosa*," *E3S Web of Conferences* 206 (2020): 02012, https://doi.org/10.1051/e3sconf/202020602012.

75. M. K. Yadav, S. Pokhrel, and P. N. Yadav, "Novel Chitosan Derivatives of 2-Imidazolecarboxaldehyde and 2-Thiophenecarboxaldehyde and Their Antibacterial Activity," *Journal of Macromolecular Science: Part A* 57 (2020): 703–710, https://doi.org/10.1080/10601325.2020.1763809.

76. M. A. Javaid, M. Rizwan, R. A. Khera, et al., "Thermal Degradation Behavior and X-Ray Diffraction Studies of Chitosan Based Polyurethane Bio-Nanocomposites Using Different Diisocyanates," *International Journal of Biological Macromolecules* 117 (2018): 762–772, https://doi.org/10.1016/j.ijbiomac.2018.05.209.

77. P. M. A. G. Araújo, P. T. A. Santos, A. C. F. M. Costa, and E. M. Araújo, "$ZnAl_2O_4$/Chitosan Films and Evaluation of the Influence of $ZnAl_2O_4$ Filler on the Films Morphology, Structure and Thermal Properties," *Materials Science Forum* 775 (2014): 692–695, https://doi.org/10.4028/www.scientific.net/MSF.775-776.692.

78. A. Abdel-Moneim, A. El-Shahawy, A. I. Yousef, S. M. Abd El-Twab, Z. E. Elden, and M. Taha, "Novel Polydatin-Loaded Chitosan Nanoparticles for Safe and Efficient Type 2 Diabetes Therapy: In Silico, In Vitro and In Vivo Approaches," *International Journal of Biological Macromolecules* 154 (2020): 1496–1504, https://doi.org/10.1016/J.IJBIOMAC.2019.11.031.

79. Y. Estévez-Martínez, R. Vázquez Mora, Y. I. Méndez Ramírez, et al., "Antibacterial Nanocomposite of Chitosan/Silver Nanocrystals/Graphene Oxide (ChAgG) Development for Its Potential Use in Bioactive Wound Dressings," *Scientific Reports* 13 (2023): 10234, https://doi.org/10.1038/s41598-023-29015-y.

80. M. Noormohammadi, M. Zabihi, and M. Faghihi, "Kinetics and Isotherms Studies on the Adsorption of Anionic Dyes and As (V) in Aqueous Solutions Employing Modified Chitosan-Alumina Nanocomposites (CSAO3 and CAO3)," *Water, Air, & Soil Pollution* 235 (2024): 48, https://doi.org/10.1007/s11270-023-06756-0.

81. J. M. Yang, C. S. Fan, N. C. Wang, and Y. H. Chang, "Evaluation of Membrane Preparation Method on the Performance of Alkaline Polymer Electrolyte: Comparison Between Poly(Vinyl Alcohol)/Chitosan Blended Membrane and Poly(Vinyl Alcohol)/Chitosan Electrospun Nanofiber Composite Membranes," *Electrochimica Acta* 266 (2018): 332–340, https://doi.org/10.1016/j.electacta.2018.02.043.

82. A. Rezaei, E. Katoueizadeh, and S. M. Zebarjad, "Investigating of the Influence of Zinc Oxide Nanoparticles Morphology on the Properties of Electrospun Polyvinyl Alcohol/Chitosan (PVA/CS) Nanofibers," *Journal of Drug Delivery Science and Technology* 86 (2023): 104712, https://doi.org/10.1016/j.jddst.2023.104712.

83. T. Remiš, P. Bělský, T. Kovářík, et al., "Study on Structure, Thermal Behavior and Viscoelastic Properties of Nanodiamond-Reinforced Poly (Vinyl Alcohol) Nanocomposites," *Polymers* 13 (2021): 1426, https://doi.org/10.3390/polym13091426.

84. X. Hong, J. He, L. Zou, Y. Wang, and Y. V. Li, "Preparation and Characterization of High Strength and High Modulus PVA Fiber via Dry-Wet Spinning With Cross-Linking of Boric Acid," *Journal of Applied Polymer Science* 138 (2021): 51394, https://doi.org/10.1002/app.51394.

85. R. A. Ilyas, H. A. Aisyah, A. H. Nordin, et al., "Natural-Fiber-Reinforced Chitosan, Chitosan Blends and Their Nanocomposites for Various Advanced Applications," *Polymers* 14 (2022): 874, https://doi.org/10.3390/polym14050874.

86. F. A. Tanjung, R. A. Kuswardani, C. I. Idumah, J. P. Siregar, and A. Karim, "Characterization of Mechanical and Thermal Properties of Esterified Lignin Modified Polypropylene Composites Filled With Chitosan Fibers," *Polymers and Polymer Composites* 30 (2022): 09673911221082482, https://doi.org/10.1177/09673911221082482.

87. R. A. O. Bernal, R. Olekhnovich, and M. Uspenskaya, "Chitosan/PVA Nanofibers as Potential Material for the Development of Soft Actuators," *Polymers* 15 (2023): 2037, https://doi.org/10.3390/polym15092037.

88. J. B. G. Jez-Campos, E. Prokhorov, G. Iuna-Bárcenas, A. Fonseca-García, and I. C. Sanchez, "Dielectric Relaxations of Chitosan: The Effect of Water on the α-Relaxation and the Glass Transition Temperature," *Journal of Polymer Science, Part B: Polymer Physics* 47 (2009): 2259–2271, https://doi.org/10.1002/polb.21823.

89. C. Lamb, *Structural Chemistry of Glasses* (Elsevier Science Ltd, 2002).

90. A. Kelly and C. Zweben, "Comprehensive Composite Materials," *Materials Today* 2 (2000): 20.

91. E. Butnaru, C. N. Cheaburu, O. Yilmaz, G. M. Pricope, and C. Vasile, "Poly(Vinyl Alcohol)/Chitosan/Montmorillonite Nanocomposites for Food Packaging Applications: Influence of Montmorillonite Content," *High Performance Polymers* 28 (2016): 1124–1138, https://doi.org/10.1177/0954008315617231.

92. K. Meera, K. Arun, and M. T. Ramesan, "Nanochitosan Reinforced Polyvinyl Alcohol/Cashew Gum Bio-Blend Nanocomposites: Promising Materials for Future Frontiers," *Journal of Polymers and the Environment* 31 (2023): 4487–4505, https://doi.org/10.1007/s10924-023-02909-8.

93. N. A. Al-Tayyar, A. M. Youssef, and R. R. Al-Hindi, "Antimicrobial Packaging Efficiency of ZnO-SiO_2 Nanocomposites Infused Into PVA/CS Film for Enhancing the Shelf Life of Food Products," *Food Packaging and Shelf Life* 25 (2020): 100523, https://doi.org/10.1016/j.fpsl.2020.100523.

94. H. R. Bakhsheshi-Rad, A. F. Ismail, M. Aziz, et al., "Development of the PVA/CS Nanofibers Containing Silk Protein Sericin as a Wound Dressing: In Vitro and In Vivo Assessment," *International Journal of Biological Macromolecules* 149 (2020): 513–521, https://doi.org/10.1016/j.ijbiomac.2020.01.139.

95. T. Koyano, N. Koshizaki, H. Umehara, M. Nagura, and N. Minoura, "Surface States of PVA/Chitosan Blended Hydrogels," *Polymer* 41 (2000): 4461.

96. T. T. Li, M. Yan, Y. Zhong, et al., "Processing and Characterizations of Rotary Linear Needleless Electrospun Polyvinyl Alcohol(PVA)/Chitosan(CS)/Graphene(Gr) Nanofibrous Membranes," *Journal of Materials Research and Technology* 8 (2019): 5124–5132, https://doi.org/10.1016/j.jmrt.2019.08.035.

97. Z. Cui, Z. Zheng, L. Lin, et al., "Electrospinning and Crosslinking of Polyvinyl Alcohol/Chitosan Composite Nanofiber for Transdermal Drug Delivery," *Advances in Polymer Technology* 37 (2018): 1917–1928, https://doi.org/10.1002/adv.21850.

98. C. Feng, K. C. Khulbe, T. Matsuura, S. Tabe, and A. F. Ismail, "Preparation and Characterization of Electro-Spun Nanofiber Membranes and Their Possible Applications in Water Treatment," *Separation and Purification Technology* 102 (2013): 118–135, https://doi.org/10.1016/J.SEPPUR.2012.09.037.

99. M. Yar, A. Farooq, L. Shahzadi, et al., "Novel Meloxicam Releasing Electrospun Polymer/Ceramic Reinforced Biodegradable Membranes for Periodontal Regeneration Applications," *Materials Science and Engineering C* 64 (2016): 148–156, https://doi.org/10.1016/j.msec.2016.03.072.

100. P. Danwanichakul and P. Sirikhajornnam, "An Investigation of Chitosan-Grafted-Poly(Vinyl Alcohol) as an Electrolyte Membrane," *Journal of Chemistry* 2013 (2013): 642871, https://doi.org/10.1155/2013/642871.

101. C. Y. Wong, W. Y. Wong, K. S. Loh, et al., "Comparative Study on Water Uptake and Ionic Transport Properties of Pre- and Post Sulfonated Chitosan/PVA Polymer Exchange Membrane," *IOP Conference Series: Materials Science and Engineering* 458 (2018): 012017, https://doi.org/10.1088/1757-899X/458/1/012017.

102. B. A. Khan, A. Khan, M. K. Khan, and V. A. Braga, "Preparation and Properties of High Sheared Poly(Vinyl Alcohol)/Chitosan Blended Hydrogels Films With *Lawsonia inermis* Extract as Wound Dressing," *Journal of Drug Delivery Science and Technology* 61 (2021): 102227, https://doi.org/10.1016/j.jddst.2020.102227.

103. N. Jain, V. K. Singh, and S. Chauhan, "A Review on Mechanical and Water Absorption Properties of Polyvinyl Alcohol Based Composites/Films," *Journal of the Mechanical Behavior of Materials* 26 (2017): 213–222, https://doi.org/10.1515/jmbm-2017-0027.

104. W. Liang, X. Liu, J. Zheng, et al., "Insight Into Crosslinked Chitosan/Soy Protein Isolate /PVA Plastics by Revealing Its Structure, Physicochemical Properties, and Biodegradability," *Industrial Crops and Products* 187 (2022): 115548, https://doi.org/10.1016/J.INDCROP.2022.115548.

105. N. H. I. Kamaludin, H. Ismail, A. Rusli, and S. S. Ting, "Thermal Behavior and Water Absorption Kinetics of Polylactic Acid/Chitosan Biocomposites," *Iranian Polymer Journal* 30 (2021): 135–147, https://doi.org/10.1007/s13726-020-00879-5.

106. Y. Han, J. Zheng, C. Jiang, F. Zhang, L. Wei, and L. Zhu, "Hydrochloric Acid-Modified Algal Biochar for the Removal of *Microcystis aeruginosa*: Coagulation Performance and Mechanism," *Journal of Environmental Chemical Engineering* 10 (2022): 108903, https://doi.org/10.1016/J.JECE.2022.108903.

107. H. S. Kim, Y. H. Park, K. Nam, S. Kim, and Y. E. Choi, "Amination of Cotton Fiber Using Polyethyleneimine and Its Application as an Adsorbent to Directly Remove a Harmful Cyanobacterial Species, *Microcystis aeruginosa*, From an Aqueous Medium," *Environmental Research* 197 (2021): 111235, https://doi.org/10.1016/J.ENVRES.2021.111235.

108. G. K. Pindihama, M. W. Gitari, R. Mudzielwana, and N. E. Madala, "Evaluating the Application of Chitosan-Based Sorbents for the Solid-Phase Adsorption Toxin Tracking of Microcystins in Irrigation Water," *Watermark* 16 (2024): 41, https://doi.org/10.3390/w16010041.

109. Y. H. Park, H. S. Kim, H. Kim, J. Park, S. Kim, and Y. E. Choi, "Direct Removal of Harmful Cyanobacterial Species by Adsorption Process and Their Potential Use as a Lipid Source," *Chemical Engineering Journal* 427 (2022): 131727, https://doi.org/10.1016/j.cej.2021.131727.

110. G. A. Magalhães-Ghiotto, J. P. Natal, L. Nishi, M. Barbosa de Andrade, R. G. Gomes, and R. Bergamasco, "Bergamasco R. Okara and Okara Modified and Functionalized With Iron Oxide Nanoparticles for the Removal of *Microcystis aeruginosa* and Cyanotoxin," *Environmental Technology* 44 (2023): 2737–2752, https://doi.org/10.1080/09593330.2022.2041105.

111. J. Sik Choi, Y. Hwan Park, S. Kim, J. Son, J. Park, and Y. E. Choi, "Strategies to Control the Growth of Cyanobacteria and Recovery Using Adsorption and Desorption," *Bioresource Technology* 365 (2022): 128133, https://doi.org/10.1016/J.BIORTECH.2022.128133.

112. Y. Peng, X. Xiao, B. Ren, et al., "Biological Activity and Molecular Mechanism of Inactivation of *Microcystis aeruginosa* by Ultrasound Irradiation," *Journal of Hazardous Materials* 468 (2024): 133742, https://doi.org/10.1016/j.jhazmat.2024.133742.

113. M. Ma, R. Liu, H. Liu, and J. Qu, "Chlorination of *Microcystis aeruginosa* Suspension: Cell Lysis, Toxin Release and Degradation," *Journal of Hazardous Materials* 217 (2012): 279–285, https://doi.org/10.1016/j.jhazmat.2012.03.030.